Ther Adv Med Oncol
2019, Vol. 11: 1–25
DOI: 10.1177/1758835919841235

Gelsolin-like actin-capping protein has prognostic value and promotes tumorigenesis and epithelial-mesenchymal transition via the Hippo signaling pathway in human bladder cancer

Lyu Zhaojie, Liu Yuchen, Chen Miao, Chen Yacun, Wu Shayi, He Anbang, Liao Xinhui, Zhang Meng, Wu Peipei, Mei Hongbing, Wang Feng, Cai Zhiming and Guan Xinyuan

Abstract

Background: Transitional cell carcinoma (TCC) of the bladder, the major histologic subtype of bladder cancer, is increasing in incidence and mortality, which requires the identification of effective biomarkers. Actin-regulating proteins have recently been proposed as important antitumor druggable targets. As a gelsolin-family actin-modulating protein, CAPG (gelsolin-like actin-capping protein) generated great interest due to its crucial effects in various biological and physiological processes; however, the role and mechanism of CAPG in TCCs remain unknown.

Materials and methods: Bioinformatic analysis and immunohistochemistry of clinical specimens were performed to detect the expression level of CAPG. Both *in vitro* and *in vivo* assays were used to determine the oncogenic effect of CAPG in TCCs. Male 4–5-week-old BALB/c nude mice were used for *in vivo* tumorigenesis assays, while SCID mice were used for *in vivo* metastatic assays. Affymetrix microarray was used to identify the underlying molecular mechanism. Western blot and immunofluorescence were used to validate the expression and localization of proteins.

Results: CAPG was frequently upregulated in TCCs and associated with clinical aggressiveness and worse prognosis. Functional assays demonstrated that CAPG could contribute to the tumorigenesis, metastasis and epithelial-mesenchymal transition (EMT) of TCCs both *in vitro* and *in vivo*. A novel mechanism that CAPG promoted TCC development *via* inactivating the Hippo pathway, leading to a nucleus translocation of Yes-associated protein was suggested.

Conclusions: The current study identified CAPG as a novel and critical oncogene in TCCs, supporting the pursuit of CAPG as a potential target for TCC intervention.

Keywords: CAPG, epithelial-mesenchymal transition (EMT), Hippo pathway, oncogene, prognosis, transitional cell carcinoma (TCC) of the bladder

Received: 18 August 2018; revised manuscript accepted: 27 February 2019.

Correspondence to:
Guan Xinyuan
Department of Clinical Oncology, Li Ka Shing Faculty of Medicine, The University of Hong Kong. Room L10-56, 10/F, Laboratory Block 21 Sassoon Road, Hong Kong State Key Laboratory of Oncology in South China and Collaborative Innovation Center for Cancer Medicine, Sun Yat-Sen University Cancer Center, 510060 Guangzhou, China
xyguan@hku.hk; lzjj.happy@163.com

Cai Zhiming
Guangdong Key Laboratory of Systems Biology and Synthetic Biology for Urogenital Tumors, Shenzhen Second People's Hospital, The First Affiliated Hospital of Shenzhen University, 518035 Shenzhen, China
caizhiming2000@163.com

Lyu Zhaojie Department of Clinical Oncology, Li Ka Shing Faculty of Medicine, The University of Hong Kong, Hong Kong, China Department of Urology, Shenzhen Second People's Hospital, The First Affiliated Hospital of Shenzhen University, Shenzhen, Guangdong, China

Liu Yuchen
Key Laboratory of Medical Reprogramming Technology, Department of Urology, Shenzhen Second People's Hospital, The First Affiliated Hospital of Shenzhen University, Shenzhen, China

Chen Miao
Wu Shayi
Department of Clinical Oncology, Li Ka Shing Faculty of Medicine, The University of Hong Kong, Hong Kong, China

Chen Yacun
Department of Pathology, The Affiliated Hospital

Introduction

Bladder cancer is the fourth most common cancer in men and one of the most significant causes of cancer-related death worldwide, with transitional cell carcinoma (TCC) being the predominant form (representing 90% of cases).[1,2] The superficial or nonmuscle-invasive TCCs, which could be managed by transurethral resection, tend to recur or progress.[3] The advanced or muscle-invasive TCCs are associated with a high risk of death from distant metastases.[4] Because of the lack of suitable diagnostic biomarkers and

of Shenzhen University, Shenzhen, China

He Anbang
Department of Urology, Peking University First Hospital, The Institute of Urology, Peking University, National Urological Cancer Center, Beijing, China

Liao Xinhui
Department of Urology, Shenzhen Second People's Hospital, The First Affiliated Hospital of Shenzhen University, Shenzhen, Guangdong, China
Department of Urology, Nanfang Hospital, Southern Medical University, Guangzhou, Guangdong, China

Zhang Meng
Department of Urology, The First Affiliated Hospital of Anhui Medical University, Hefei, Anhui, China

Wu Peipei
Department of Respiratory and Critical Care, The First Affiliated Hospital of Anhui Medical University, Hefei, Anhui, China

Mei Hongbing
Wang Feng
Department of Urology, Shenzhen Second People's Hospital, The First Affiliated Hospital of Shenzhen University, Shenzhen, Guangdong, China

effective therapies, patients are often diagnosed at advanced stages and the mortality rate keeps increasing.[5] Considering these issues, it is essential to study TCCs at the genetic level to characterize the targeted agents.

The improvement in high-throughput sequencing and big data mining with bioinformatics have provided enormous insights into the genomic landscape and identified new biomarkers in TCCs.[6] Sequencing of bladder cancer has identified recurrent mutations in *TP53, FGFR3, TSC1, PIK3CA, RB1* and *HRAS*.[7] In recent years, our team have performed large-scale whole-genome and whole-exome sequencing of TCCs, which identified genetic alterations in the sister chromatid cohesion and segregation and chromatin-remodeling processes as key hallmarks of TCCs.[8–10] Notwithstanding, the value of these emerging genes in TCC remains largely unknown, which merits further exploration and better understanding.

The gelsolin-like actin-capping protein CAPG (also known as macrophage-capping protein, AFCP, HEL-S-66, and MCP), is a calcium-sensitive actin-binding protein regulating cytoplasmic and nuclear structures.[11] The gelsolin protein superfamily is an evolutionarily conserved family of proteins present among species. As a member of the ubiquitous gelsolin family, CAPG is distinguished from other gelsolin proteins through unique features.[12] CAPG has only three repeated gelsolin-like domains, in contrast with the usual six domains, which probably leads to the lack of actin-severing activity of CAPG exhibited by the other family members.[11] The subcellular localization is another distinct feature of CAPG. It localizes to both the nucleus and cytoplasm, whereas the other gelsolin family members only present in the cytoplasm.[13] The nuclear section of CAPG is reported to be involved in phosphatidylinositol-driven chromatin remodeling[14,15] and transcriptional regulation,[16] mainly through actin nucleation and assembly.[17] The cytoplasmic CAPG, on the other hand, caps the end of actin filaments in a Ca^{2+} and phosphatidylinositol 4,5-bisphosphate-dependent (PIP2) manner. In addition, CAPG has been shown to regulate the actin cytoskeleton restructuring and cellular migrating in fibroblastic cells and endothelial cells.[18,19]

CAPG plays a crucial role in normal cells. More importantly, the deregulation of CAPG could result in cellular malignant changes.[20,21] Through exploring the Cancer Genome Atlas (TCGA) data, we found frequent upregulation of CAPG in most cancers, especially in TCCs. However, the effects of CAPG in TCCs have not been illustrated to date. The current study set out to evaluate CAPG expression and its clinical significance and prognostic value. Secondly, we examined the biological effects of CAPG in malignant features of TCCs, both *in vitro* and *in vivo*. For this purpose, we selected nude mice (which harbor the genetic mutant resulting in a lack of body hair and an inhibited immune system) as a xenograft model in tumorigenesis experiments. While the SCID ('severe combined immune deficiency') mice, with neither mature B nor T-cells, are used for the tumor metastasis model.[22,23] Thirdly, we explored the oncogenic mechanisms of CAPG in the development of TCCs. It is noteworthy that this study will further our understanding of TCCs as well as provide a potential therapeutic and prognostic target for this disease.

Materials and methods

Big data analysis

Illumina RNA Sequencing (version 2) transcriptome data and clinical characteristics of 413 cases with TCCs were retrieved from TCGA (http://cancergenome.nih.gov/) and the cBioPortal (http://www.cbioportal.org) in January 2018.[24,25] All provisional datasets were analyzed for CAPG expression, mutation, somatic copy-number alterations, clinicopathologic and survival analysis. The profile of CAPG was further analyzed in the Gene Set Enrichment Analysis (GSEA; 2.2.1, http://www.broadinstitute.org/gsea) to determine which pathway may be involved in CAPG-mediated TCC progression. GSEA software of the present study used 'Hallmark gene sets [h.all.v5.2.symbols.gmt (Hallmarks)]' as the gene sets to be analyzed. We additionally searched for CAPG expression and copy-number variation in Oncomine (https://www.oncomine.org/resource/login.html) across all available datasets (updated January 2018).[26]

Immunohistochemistry

A total of 101 paraffin-embedded TCC samples with 101 paired nontumor tissues from patients who underwent transurethral resection, partial cystectomy or radical cystectomy of TCCs at Sun Yat-Sen University Cancer Center (Guangzhou,

China) between 2000 and 2014 were used in this study. None of the patients received preoperative treatment. Clinicopathological classification and staging were carried out by pathologists, according to criteria of the American Joint Committee on Cancer. Informed patient consent and approval from the Institutional Research Ethics Committee at Sun Yat-Sen University Cancer Center (Guangzhou, China) were obtained for the research use of these clinical materials (approval no.: GZR2015-311). All procedures performed in studies involving human participants were in accordance with the ethical standards of the institutional or national research committee and with the 1964 Helsinki Declaration.

The immunohistochemistry (IHC) procedure and scoring of CAPG expression were performed as per the standard protocol.[27] Briefly, sections adhered to slides were deparaffinized with xylene and rehydrated prior to antigen retrieval by microwaving in sodium citrate buffer (pH 6.0). The sections were then incubated with primary antibody at 4℃ overnight. The antibodies used in IHC included CAPG (1:300 dilution, Sigma, MO, USA, HPA019080) and Ki67 (1:200 dilution, Abcam, CT, USA, ab15580). After washing with phosphate-buffered saline (PBS) three times, sections were incubated with a secondary antibody (1: 100 dilution, Santa Cruz, CA, USA) for 30 min at room temperature. The DAB substrate kit (DAKO, Carpinteria, CA, USA) was used for signal development, then they were counterstained by Mayer's hematoxylin, dehydrated, and mounted. Each slide was assessed by two pathologists independently. The score of CAPG expression was calculated as tumor cell staining multiplied by the score of staining intensity. The semiquantitative grading system was adopted as previously described.[28] Briefly, tumor cells staining was assigned a score using a six-category (0–5) grading system according to the percentage of stained tumor cell numbers. The stain intensity was scored as: 0, nonstaining; 1, weak staining; 2, moderate staining; and 3, strong staining. Consensus was established by reviewing the slides together. A third pathologist intervened and evaluated the discrepant cases. The complete TCC specimen IHC results were divided into four degrees: 'CAPG−' showing a complete lack of staining; 'CAPG +' showing faint, barely discernible staining; 'CAPG++' showing readily recognizable positivity but to a lesser extent staining and 'CAPG+++' showing widespread, intense staining.

Cell lines and cell culture

All TCC cell lines 5637, T24, SW780, TCCSUP, RT-4, HT1197 and the immortalized normal bladder cells SV-HUC-1 were purchased from American Type Culture Collection in 2017. All cells were cytogenetically tested and authenticated before the cells were frozen. T24 cells were cultured in McCoy's 5A medium with 10% fetal bovine serum (FBS). A total of 5637 cells were cultured in Roswell Park Memorial Institute (RPMI) 1640 supplemented with 10% FBS. SV-HUC-1 cells were cultured in Dulbecco's modified eagle medium (DMEM)/F-12 media with 10% FBS. Other cells were cultured in DMEM with 10% FBS. Cell plates were placed at 37℃ in a fully humidified incubator of 5% CO_2 in air.

Animals

The animal experiment was performed under HK Animals Ordinance license (no. of license: 16-990 in DH/HA & P/8/2/3 Pt.91) according to standard policies. The experimental protocol was approved by the University of Hong Kong Animal Welfare Committee (approval no.: CULATR-4090-16). All procedures were made to minimize the suffering and number of animals in compliance with the ethical standards of the institutional or national research committee. All animals used in this study were ordered from the Laboratory Animal Unit of the University of Hong Kong. All the mice were kept in standard cages at 26 ± 1°C under a 12/12 h light/dark cycle and fed the rodent standard diet with free access to water. The mice were randomly divided into control groups or experimental groups, with each group containing six mice.

For the *in vivo* tumorigenic study, we used 4–5-week-old male BALB/c nude mice (mean body weight: 15.5 ± 1.2 g), which were housed under standard conditions and cared for according to the institutional guidelines for animal care.[29] Control cells (SW780-Vec, 5637-shCtrl and T24-shCtrl) and CAPG-overexpressing or CAPG-knockdown cells (SW780-CAPG, 5637-shCAPG and T24-shCAPG) were subcutaneously injected into the right dorsal flank of nude mice in a laminar flow cabinet. The cell number injected into each mouse was 5×10^6 which were suspended in 150 µl PBS. The length (L) and width (W) of tumors were measured by calipers once every week and tumor volume was calculated by the formula $V = 0.5 \times L \times W^2$.[30]

After continuous observation for 6 weeks, mice were sacrificed, and tumors were excised, measured and collected for future pathological studies. For the mechanism study, in order to assess the effects of Yes-associated protein (YAP) inhibition *in vivo*, the nude mice were firstly subcutaneously injected with SW780-CAPG cells (5×10^6 / left flank and 1×10^7 /right flank). Then six mice were randomly chosen and injected with verteporfin (VP), the Hippo/YAP inhibitor (Sigma, 129497-78-5) once every other day starting from week 3 to week 5 in the dosage of 80 mg/kg intraperitoneally according to previous study.[31] The other six mice were treated with dimethyl sulfoxide (DMSO) in the same manner. After 6 weeks, mice were sacrificed, and tumors were removed, measured and collected for IHC staining to detect YAP (CST, #13008) expression.

For the metastatic model, we firstly infected SW780-CAPG and SW780-Vec cells with luciferase lentivirus. A total of 1×10^6 SW780-CAPG-luciferase cells or SW780-Vec-luciferase cells were suspended in 100 µl sterile PBS and then injected into the tail vein of a 5-week old SCID mouse. A total of six mice were used for each group. Bioluminescent images were taken on the first day of injection and also every week after cell implantation to detect the tumor migration. After 5 weeks from the cell injection, mice were sacrificed, and the lungs were collected. The weight of the lungs and visible metastatic tumor nodules on the surface of the lungs were quantified.

CAPG overexpression and knockdown

The full-length wildtype CAPG cDNA (NM_001256139.1) was cloned (forward primer: 5' - ATGTACACAGCCATTCCCCA-3' and reverse primer:5'- TCATTTCCAGTCCTTG AAAAA TTGC-3') into the pCDH-cmv-mcs-EF1-Puro expression vector (Biosciences). Empty vector-transfected cells were used as controls (Vec). To inhibit CAPG expression efficiently, small interfering RNA specifically targeting CAPG was designed (sequences: 5′-TGATAT CTGATG ACTGCTT-3′) and transformed into short hairpin RNA (shCAPG). The sequence of scrambled shRNA (5′-TTCTCCGAACGTG TCACGT-3′) was used as negative control (shCtrl). To generate the lentivirus, vectors were inserted into the Lentivector Expression Systems (GeneChem, China) and then transfected into HEK 293T cells using Lipofectamine 2000 (Invitrogen, USA) according to the manufacturer's instructions. After 72 h of incubation, the lentivirus particles were harvested from the transduced 293T cells, followed by the transfection to targeted TCC cells using polybrene (Sigma, USA). Stable clones were selected using puromycin (Sigma-Aldrich).

Quantitative real-time polymerase chain reaction

Total RNA was extracted from the cells using the TRIzol reagent (Invitrogen) as per the manufacturer's procedures. The reverse transcription of cDNA was performed using a Reverse Transcription polymerase chain reaction (RT-PCR) kit (Roche). Quantitative RT-PCR was performed in triplicate using SYBR Green PCR kit (Applied Biosystems) and ABI PRISM 7900 Sequence Detector (Applied Biosystems). Glyceraldehyde 3-phosphate dehydrogenase (GAPDH) expression was used as an internal control. Primers were synthesized by Invitrogen (CAPG, 5′-GCAGCTCTGT ATAAGGTCTCTG-3′ and 5′-TTTCGCCCCT TCCAGATATAG-3′; GAPDH, 5′-TGACTTC AACAGCGACACCCA-3′ and 5′-CACCCTGT TGCTGTAGCCAAA-3′; forward and reverse). All results were expressed as fold changes in mRNA expression with respect to the control cells and the data were interpreted using the $2^{-\Delta\Delta Ct}$ method.

Western blot

Total protein was isolated from treated cells which were washed twice with PBS, harvested, and lysed with ice-cold protein lysis buffer [1 M Tris-HCl, pH = 6.8, 100 mM; 2% mercaptoethanol; 20% glycerin; 4% sodium dodecyl sulfate (SDS)]. Protein concentration level was measured using the BCA protein assay kit (Pierce, USA). Then the total 20 µg protein was loaded onto a gel electrophoresis SDS-polyacrylamide gel electrophoresis and transferred onto a polyvinylidene difluoride membrane. The antibodies used for immunoblotting included CAPG (Sigma, HPA019080), GAPDH (CST, #5174), E-cadherin (CST, #3195), β-catenin (CST, #8480), vimentin (CST, #5741), N-cadherin (CST, #13116), Hippo signaling antibody sampler kit (CST, #8579) and the secondary antibody goat anti-mouse immunoglobulin (Ig)G horseradish peroxidase (HRP; Sigma-Aldrich, A4416) and goat anti-rabbit IgG HRP antibody (Sigma-Aldrich, A9169).

Immunofluorescence

Immunofluorescence (IF) staining was performed on TCC cells. Briefly, cells were seeded on coverslips at 50% confluence and fixed by 4% paraformaldehyde for 10 min and permeabilized in PBS with Tween (PBS-T; 0.05% Triton X-100) for 10 min. After blocking in 5% bovine serum albumin for 30 min at room temperature, the cells were incubated with primary antibodies at 4°C overnight. After washing three times in PBS, cells underwent incubation with secondary antibodies in a dark humidified chamber for 1 h at room temperature. The nucleus was stained by 4',6-diamidino-2-phenylindole (DAPI; Invitrogen, CA, USA). The images were visualized under Carl Zeiss LSM700 fluorescence microscope (Zeiss, Germany) and analyzed using ImageJ software (National Institutes of Health, Bethesda, MD, USA).

Cell proliferation assays

An XTT assay (Roche Applied Science, Germany), Celigo Imaging cell cytometer (Nexcelom, USA) and foci formation assay (Sigma-Aldrich) were used according to the manufacturer's instructions. For a standard vitality XTT assay, each cell line was cultured in 96-well plates at a density of 2×10^3 cells per well. After adding XTT reagent (20 μl per well, 5 mg/ml), cells were incubated at 37°C for 2 h. The cell growth rate was then measured by detecting the absorbance value through a spectrophotometer (Tecan Sunrise, Switzerland) using a measure wavelength of 490 nm. Cell viability was monitored daily for total 5 days. Overall, three independent experiments were performed and each was done in triplicate. Another cell proliferation test was examined by using the Celigo Imaging cell cytometer. TCC cells were plated at 2000 cells/well in 96-well plates in the complete medium at 37°C with 5% CO_2 in air on day 1. The number of cells in each well was counted daily from day 2 to day 5. The proliferation rate was expressed as a ratio of the cell counts on days 2–5 normalized against day 1. For the foci formation assay, $1–3 \times 10^3$ cells were plated in each well of a six-well plate. After 7–10 days culture, surviving colonies were fixed with 100% ethanol and counted with crystal violet staining. Overall, three independent experiments were performed. The foci numbers were calculated by ImageJ software (National Institutes of Health).

Cell apoptosis assays

To detect cell apoptosis, Annexin V-APC apoptosis detection kit (eBioscience, USA) was used following the manufacturer's protocol. After treatment, cells were re-suspended at a concentration of 1×10^6/ml in 200 μl binding buffer (1×). Then 5 μl Annexin V-APC was added to each 100 μl cell suspension. The cells were mixed and incubated at room temperature for 15 min and then analyzed by flow cytometry (FACS; Millipore, Guava easyCyte HT). The experiment was performed three times. Apoptotic cells were also detected using Caspase-Glo 3/7 assay kit (Promega, USA). Briefly, cells were re-suspended in 100 μl of culture medium and mixed with 100 μl of caspase substrate. Lysates of cells were diluted to a concentration of 1×10^4 cells/well and incubated for 4 h at room temperature. The fluorescence was measured with an excitation wavelength of 485 nm and an emission wavelength of 530 nm under the fluorescence microscope (Olympus, IX71).

Cell migration and invasion assays

A wound-healing assay was used to determine the cell mobility. Briefly, cells were cultured in a six-well plate. The culture medium was replaced by serum-free medium 24 h before a wound scratch. After wounding by a sterile tip, the medium was changed to remove cellular debris. Serial photographs were taken at different time points. In addition, migration and invasion assays were conducted in the 24-well Transwell Chambers (Corning, USA) or the Matrigel BioCoat Invasion Chambers (Corning, USA). Briefly, cells were seeded into the upper chambers at the density of 1×10^5 cells per well and cultured in 500 μl serum-free medium at 37°C for 1 h. Then 700 μl medium containing 30% FBS was added to the lower chamber and then incubated at 37°C for 24 h or 48 h. Cells transmigrating the membrane or invading through Matrigel were fixed, stained with crystal violet and counted using an inverted phase contrast microscope and photographed (Cikong, XDS-100).

Microarray procedure

The quality of total RNA samples was assessed by Nanodrop 2000 (Thermo Scientific, MA, USA) and Aglient 2100 Bioanalyzer (Agilent Technologies, CA, USA). Total RNA was isolated 48 h after transfection and analyzed by using

the GeneChip Primeview Human Gene Expression Arrays (Affymetrix, USA). Briefly, the Affymetrix GeneChip 3'IVT Express kit was used for cDNA target preparation. The fragmented and labeled cDNA was generated and hybridized onto Human Gene 1.0 ST arrays in Affymetrix GeneChip Hybridization Oven 645. Arrays were washed, stained and processed using Affymetrix GeneChip Fluidics Station 450 systems. Then they were imaged using an Affymetrix GeneChip Scanner 3000 for the subsequent generation of raw data.

Ingenuity Pathway Analyses

Ingenuity Pathway Analyses (IPA) software (Qiagen, USA) was performed to reveal the canonical pathways, upstream transcriptional regulators, biological processes and molecular networks following CAPG upregulation. The list of differentially expressed genes, containing gene identifiers and corresponding expression values, was uploaded into IPA. Every gene identifier was mapped to its corresponding gene object in the Ingenuity Pathway Knowledge Base (IPKB). Canonical pathway analysis was used to identify networks from the IPA library that were most significantly modulated across anatomical sites. Functional enrichment analysis identified the biological functions or diseases that were most significant to the data set. The likeliness that a group of the candidate genes is involved in a represented function is measured by the significance value. The significance of the association between each data set and specific pathways or functions, was determined in three ways: (1) A p value calculated by Fisher's exact test to determine the probability of the association between genes in the dataset and the pathway of interest; (2) A z-score inferring the overall activation or inhibition states of functions caused by transcriptional regulators; and (3) a ratio calculated by the molecule's number from the dataset mapped to the pathway *versus* the total molecules' number mapped to the IPKB pathway.

Statistical analysis

IBM SPSS Statistics 19 software (SPSS, Chicago, IL, USA) was applied to perform statistical analysis in current study. A two-tailed Chi-square test was used to analyze the association of CAPG expression in patients with TCCs with different clinicopathological features. A Kaplan–Meier plot and log-rank test were used for survival analysis. Both univariate and multivariate Cox proportional hazard regression models were used to examine independent prognostic predictor variables. A Student's t test was applied to assess the statistical significance between two preselected groups. The one-way analysis of variance (ANOVA) was used to determine the significant differences between two or more independent groups. The data are presented as the mean ± standard deviation (SD) of three independent experiments. The p values are denoted as $^{*}p < 0.05$, $^{**}p < 0.01$, $^{***}p < 0.001$ in all figures.

Results

CAPG is frequently upregulated in TCCs and correlated with poor prognosis

We systematically analyzed CAPG mRNA expression in 20 cancer types using the latest RNA sequencing dataset from TCGA and identified that CAPG was significantly upregulated in 13 cancer types, for example, thyroid cancer, breast cancer (BRCA) and bladder cancer (BLCA) as shown in Figure 1(a). We also searched for CAPG in Oncomine and found CAPG was upregulated in infiltrating or superficial bladder carcinoma compared with normal bladder tissues ($p < 0.001$) [Figure 1(b)]. To exclude the influence of differences between individuals, we further compared the mRNA levels in 19 paired TCC tissues *versus* the matched-pair normal tissues from TCGA and found that CAPG was significantly upregulated in TCC samples [$p = 0.0077$; Figure 1(c)].

To determine CAPG protein expression in human TCCs, we performed IHC staining of CAPG on 101 paraffin-embedded archived human TCC and their paired normal samples with a CAPG-specific antibody. The representative images of the IHC staining with various levels of CAPG expression are presented. In general, immunostaining of CAPG in malignant samples were stronger than the benign tissues. Statistical analysis confirmed the enhanced staining of CAPG in malignant samples: 89.1% of the tumor specimens (90/101) displayed positive staining and nearly one-quarter of them (20/90, 22.2%) presented widespread and intense staining (CAPG +++), whereas its expression was absent (CAPG−) in almost half of nontumor samples [50/101, 49.5%; Figure 1(d)].

Then we explored the prognostic significance of CAPG. In a Kaplan–Meier survival analysis using

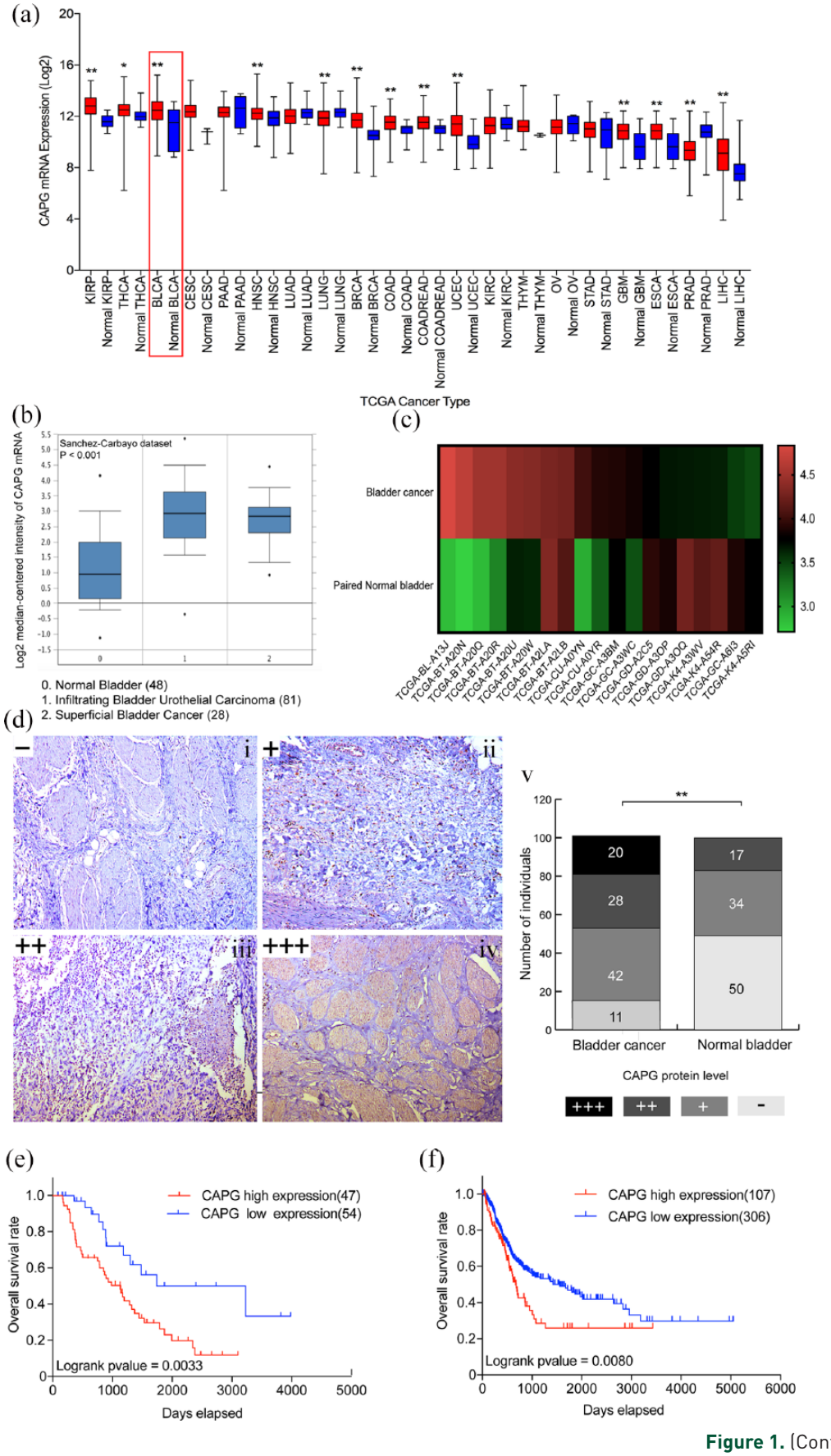

Figure 1. (Continued)

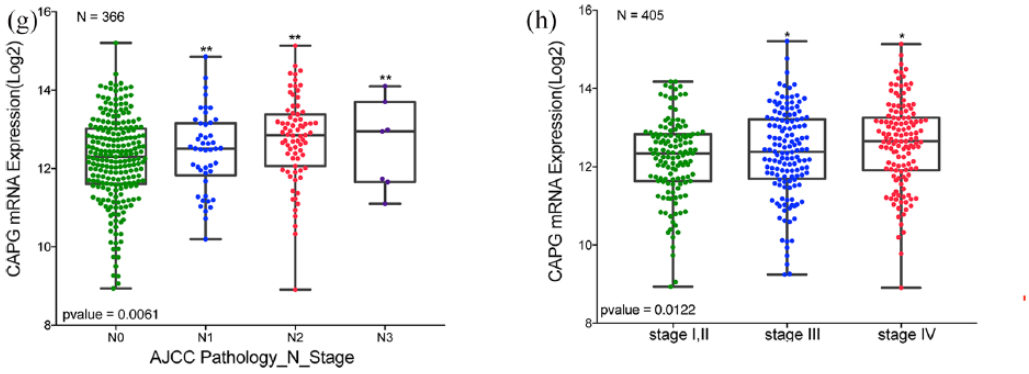

Figure 1. CAPG is frequently upregulated and correlates with poor overall survival in TCCs. (a) The landscape of CAPG mRNA expression in various human cancers compared with normal tissues from TCGA (dated June 2018). *$p < 0.05$, **$p < 0.01$. (b) CAPG mRNA is frequently upregulated in TCCs as revealed by Oncomine data-mining analysis (Sanchez-Carbayo dataset). (c) CAPG mRNA expression (RNA-Seq V2 RSEM, log2) is significantly higher in 19 tumor samples than the paired nontumor margin tissues analyzed based on TCGA datasets ($p = 0.0077$). (d) IHC analysis of the expression of CAPG protein in TCCs. CAPG is localized both within the nuclei and cytoplasm. (i) IHC staining of the adjacent normal tissues is mainly negative (CAPG–). (ii–iv) The staining of tumor tissues is mostly positive. (ii) Weak staining (CAPG+); (iii) Moderate staining (CAPG++); (iv) Strong staining (CAPG+++). (100× magnification) (v) Bar chart shows the summary of the distribution of different CAPG protein levels in tumor *versus* nontumor for all paired cases ($n = 101$). **$p < 0.01$. (e and f) Kaplan–Meier survival curves show that high CAPG expression is significantly associated with poor overall survival in patients from (e) 101 informative TCC cases ($p = 0.0033$) and (f) TCGA dataset ($p = 0.0080$). (g and h) Dot plots show that high CAPG expression is correlated with (g) high pathologic N grade ($p = 0.0061$, $n = 366$) and (h) advanced tumor stages ($p = 0.0122$, $n = 405$).
CAPG, gelsolin-like actin-capping protein; IHC, immunohistochemistry; TCC, transitional cell carcinoma; TCGA. the Cancer Genome Atlas.

these 101 informative TCC samples, high CAPG expression was significantly associated with short survival time (log-rank test, $p = 0.0033$). Another survival analysis based on TCGA cases ($n = 413$) confirmed that high CAPG expression was a significant predictor for worse outcome of TCCs (log-rank test, $p = 0.0080$). In a multivariate Cox regression analysis, CAPG was further validated as an independent prognostic factor for the overall survival of TCCs [hazard ratio (HR) =1.553, 95% confidence interval (CI): 1.288–2.954, $p < 0.001$; Table 1].

The clinicopathologic association study in our clinical samples showed that CAPG overexpression was significantly correlated with family medical history (Pearson Chi-square test, $p = 0.0432$), lymph node metastasis (Pearson Chi-square test, $p = 0.0077$), and high pathological stage (Pearson Chi-square test, $p = 0.0003$), yet not with age, sex, tobacco smoking and pathologic T and M grades (Table 2). To further validate the clinical significance of CAPG in TCCs, we analyzed the clinical characteristics in TCGA database and found that CAPG upregulation was associated with lymph node spread [$p = 0.0061$, $n = 366$; Figure 1(g)] and advanced pathologic stages [$p = 0.0122$, $n = 405$; Figure 1(h)].

Upregulation is a common feature of oncogenes, which can be caused by mutation, gene amplification, and translocation.[32] We further examined CAPG gene alterations in TCGA datasets using cBioPortal. Notably, among all cancer types with TCGA data, the CAPG gene was most frequently amplified in TCCs [*BLCA*; Supplementary Figure 1(a)]. To study whether CAPG copy-number status correlated with the mRNA expression, we found a significant association between increased CAPG expression and DNA copy-number amplification in TCGA BLCA database [Supplementary Figure 1(b)]. We additionally observed an obvious increase in CAPG gene copy number in TCCs compared with normal tissue or blood from the Oncomine database [Supplementary Figure 1(c)].

CAPG has a strong oncogenic function in TCCs

To further explore the function of CAPG contributing to malignancies of TCCs, the expression of CAPG was detected in one immortalized cell line

Table 1. Univariate and multivariate OS analysis of various prognostic parameters for patients with TCC by the Cox proportional hazard model.

Variables	Univariate analysis		Multivariate analysis	
	Hazard ratio for OS (95% CI)	*p* value	Hazard ratio for OS (95% CI)	*p* value
Age (⩾60 *versus* <60)	1.034 (1.015–1.174)	0.2400	1.178 (0.815–1.602)	0.2911
Sex (female *versus* male)	1.505 (1.211–1.980)	0.1300	1.421 (0.920–2.384)	0.0667
Surgical method (cystectomy *versus* transurethral resection)	1.130 (0.667–1.934)	0.0156*	1.739 (1.018–2.972)	0.0428*
Pathologic stage (III/IV *versus* I/II)	1.169 (0.998–2.755)	0.0017**	1.280 (1.177–3.366)	0.0012**
Pathologic N (N1,2,3 *versus* N0)	2.334 (1.301–4.187)	0.0374*	3.022 (2.379–4.536)	0.0303*
Pathologic M (M1 *versus* M0)	1.209 (0.525–2.784)	0.6560	1.093 (0.673–2.502)	0.3844
CAPG expression (high *versus* low)	1.387 (1.139–2.464)	<0.001***	1.617 (1.335–3.121)	<0.001***

* $p < 0.05$, ** $p < 0.01$, ***<0.001.
CAPG, gelsolin-like actin-capping protein; CI, confidence interval; OS, overall survival; TCC, transitional cell carcinoma.

(SV-HUC-1) and six TCC cell lines through Reverse Transcription-Ploymerase Chain Reaction (RT-PCR), quantitative Real-time Ploymerase Chain Reaction (qRT-PCR) and western blot [Figure 2(a)]. SW780 cells with the lowest CAPG expression were selected for a gain-of-function study. We firstly transfected the lentivirus packaged with either a CAPG-expressing vector or an empty vector control to generate CAPG-overexpressing (SW780-CAPG) or control cells (SW780-Vec). Then we chose T24 and 5637 cell lines with higher expression level of CAPG than other cells for the loss-of-function study. They were stably transduced with either CAPG-specific short hairpin RNA (shCAPG) lentivirus or a non-target control (shCtrl) to generate cells with CAPG repressed or control cells. Successful ectopic expression and effective knockdown of CAPG were validated in both mRNA and protein levels by qRT-PCR and western blot, respectively [Figures 2(b) and 3(a)].

The tumorigenic potential of CAPG was assessed by cell proliferation assays including XTT assay, foci formation assay, Celigo assay and xenograft tumor formation study (Figures 2 and 3). With respect to the control group, the cellular proliferative rate of SW780-CAPG cells were remarkably enhanced in XTT assay [Figure 2(c)] as well as in Celigo system [Figure 2(d)]. Similarly, more foci were yielded in CAPG-upregulated cells in the foci formation assay [Figure 2(e)]. Consistent with *in vitro* result, xenograft tumors formed by SW780 cells transfected with CAPG was significantly larger in the mean volume than tumors induced by vector control, as indicated by the final xenograft tumor volume and the tumor growth curves [Figure 2(h)]. IHC staining of the xenograft tumors confirmed higher expression of CAPG and Ki67 protein in the tumors formed by CAPG transfected cells than those of the vector control cells [Figure 2(h, e and f)].

Conversely, the knockdown of CAPG expression revealed an opposing effect both *in vitro* and *in vivo*. A significant impairment of cell growth and a reduction of foci numbers were induced by the knockdown of CAPG in T24 and 5637 cells compared with their control counterparts [Figure 3(b, c and d)]. *In vivo*, T24-shCAPG and 5637-shCAPG cells had a significantly decreased ability to form tumors in nude mice compared with vector-transfected cells. The expression of CAPG and Ki67 protein was decreased in tumors formed by T24-shCAPG and 5637-shCAPG cells than their counterparts [Figure 3(g)]. Hence, these data demonstrated that CAPG has a strong tumorigenic ability both *in vitro* and *in vivo*.

CAPG could also inhibit apoptosis in TCC cells. We observed a significant decrease in the number of apoptotic cells using flow cytometry assays

Table 2. The clinicopathologic characteristics of the 101 patients and the association with CAPG expression.

Variables	Total (cases)	Expression		*p* value
		Low (54 cases)	High (47 cases)	
Age group				0.6635
<60	60	31	29	
⩾60	41	23	18	
Sex				0.0903
Female	20	14	6	
Male	81	40	41	
Family medical history				0.0432*
No	43	28	15	
Yes	58	26	32	
Tobacco smoking				0.8537
Smoker	42	22	20	
Nonsmoker	59	32	27	
Surgical method				0.0694
Transurethral resection	32	22	10	
Partial cystectomy	26	14	12	
Radical cystectomy	43	18	25	
Pathologic T				0.2294
T0	2	1	1	
T1	2	1	1	
T2	49	32	17	
T3	20	9	11	
T4	28	11	17	
Pathologic M				0.0866
M0	55	29	26	
M1	19	14	5	
MX	27	11	16	
Pathologic N				0.0077**
N0	36	11	25	
N1	37	25	12	
N2	19	12	7	
N3, NX	9	6	3	
Pathologic stage				0.0003***
Stage I, II	41	31	10	
Stage III	24	12	12	
Stage IV	36	11	25	

* $p < 0.05$, ** $p < 0.01$, *** $p < 0.001$; p value was calculated by a Chi-square test.
CAPG, gelsolin-like actin-capping protein.

after overexpression of CAPG in SW780 cells compared with the control. The caspase 3/7 activity was also downregulated by CAPG upregulation [Figure 2(f and g)]. Conversely, as shown in Figure 3(e) and (f), the apoptosis rates of the T24 and 5637 cells in shCAPG groups were significantly higher than the negative control group. The caspase 3/7 activity were upregulated in T24 and 5637 cell lines treated with shCAPG lentivirus compared with the shCtrl group.

CAPG promoted TCCs metastasis as an EMT-inducing factor

Several studies have showed that CAPG is involved in the control of actin-based cell motility of benign cells and malignant cells.[20,21] Furthermore, the analysis of big data and TCC clinical specimen indicated that overexpression of CAPG was associated with lymph node metastasis and tumor stage progression. These evidences raise the possibility that CAPG also plays an important role in facilitating TCCs metastasis. Therefore, we investigated whether CAPG could promote migration and invasion capacity in TCC cells. After establishing the stable CAPG-upregulated SW780 cells and CAPG-downregulated 5637 cells as previously described, a CAPG plasmid was transfected to the CAPG-downregulated 5637 cells to re-overexpress the CAPG gene and the shRNA plasmid was transfected to the CAPG-upregulated SW780 cells to re-knockdown the CAPG gene. The CAPG expression in mRNA and protein levels are shown [Figure 4(a i and ii)]. In the wound-healing assays, the CAPG gene expression was increased by 519 % and enhanced the migration rate by 174% in the SW780-CAPG group compared with the SW780-Vec group, while the CAPG level fell by 218% and exhibited a decrease in the migration rate of 88% in the SW780-CAPG-shCAPG group compared with SW780-CAPG group [Figure 4(b)]. For 5637 cells, the CAPG-knockdown group showed a 75% decrease in CAPG expression and exhibited obvious inhibition in migration rate compared with the control group, while the CAPG-re-overexpressed cells were demonstrated to reverse its migration ability significantly [Figure 4(c)]. Transwell assay analysis revealed similar promoting effects of CAPG in SW780 and 5637 cells on cell migration and invasion [Figure 4(d and e)]. The results above showed that an increase of CAPG expression can significantly enhance cancer migration/invasion in TCCs and vice versa.

To directly assess whether CAPG promotes metastasis *in vivo*, we intravenously injected SW780-CAPG-luciferase cells and SW780-Vec-luciferase cells through the tail vein six SCID mice for each group (1×10^6 cells/100 μl PBS/mouse). Bioluminescent images were taken on the first day of injection and weekly after cell implantation till 5 weeks. Consistent with the results of functional studies *in vitro*, CAPG-overexpression cells exhibited an increased lung weight and lung nodules at 35 days post-injection than the control group, implying that CAPG is critical for the colonization of TCCs cells in lung. The IHC analyses disclosed a high number of metastatic colonies formed by SW780-CAPG cells compared with the control group, which supported the macroscopic observations [Figure 4(f)].

In order to investigate the potential mechanisms by which CAPG accelerates TCC metastasis, GSEA was performed based on the RNA-seq data from TCGA BLCA database. Among the analysis results, EMT which is believed as a key event for tumor metastasis, was significantly enriched in high CAPG expression group compared with the low CAPG expression group [Figure 4(g)]. To further validate the EMT-promoting capability of CAPG, we next evaluated the EMT-associated marker genes. Western blot assays presented that the expression of epithelial markers (E-cadherin and beta-catenin) were downregulated, whereas the mesenchymal markers (vimentin and N-cadherin) were upregulated in CAPG-overexpressing SW780 cells compared with their counterparts. In contrast, the CAPG-knockdown 5637 cells tended to exhibit more epithelial characteristics than mesenchymal characteristics compared with the control group [Figure 4(h)]. To intuitively describe these changes, IF detection was performed. Consistent with the western blot results, SW780-CAPG cells displayed a weaker red fluorescence in cell membrane stained with E-cadherin and β-catenin antibodies, while a stronger red fluorescence when stained with vimentin and N-cadherin antibodies compared with the SW780-Vec cells [Figure 4(i)]. These findings evidently demonstrated that CAPG promotes TCCs metastasis by inducing EMT.

CAPG inactivates Hippo signaling leading to YAP activation

In an attempt to determine the mechanisms underlying CAPG-mediated TCCs development and progression, we sought to compare the transcriptome of SW780 cells transfected with CAPG

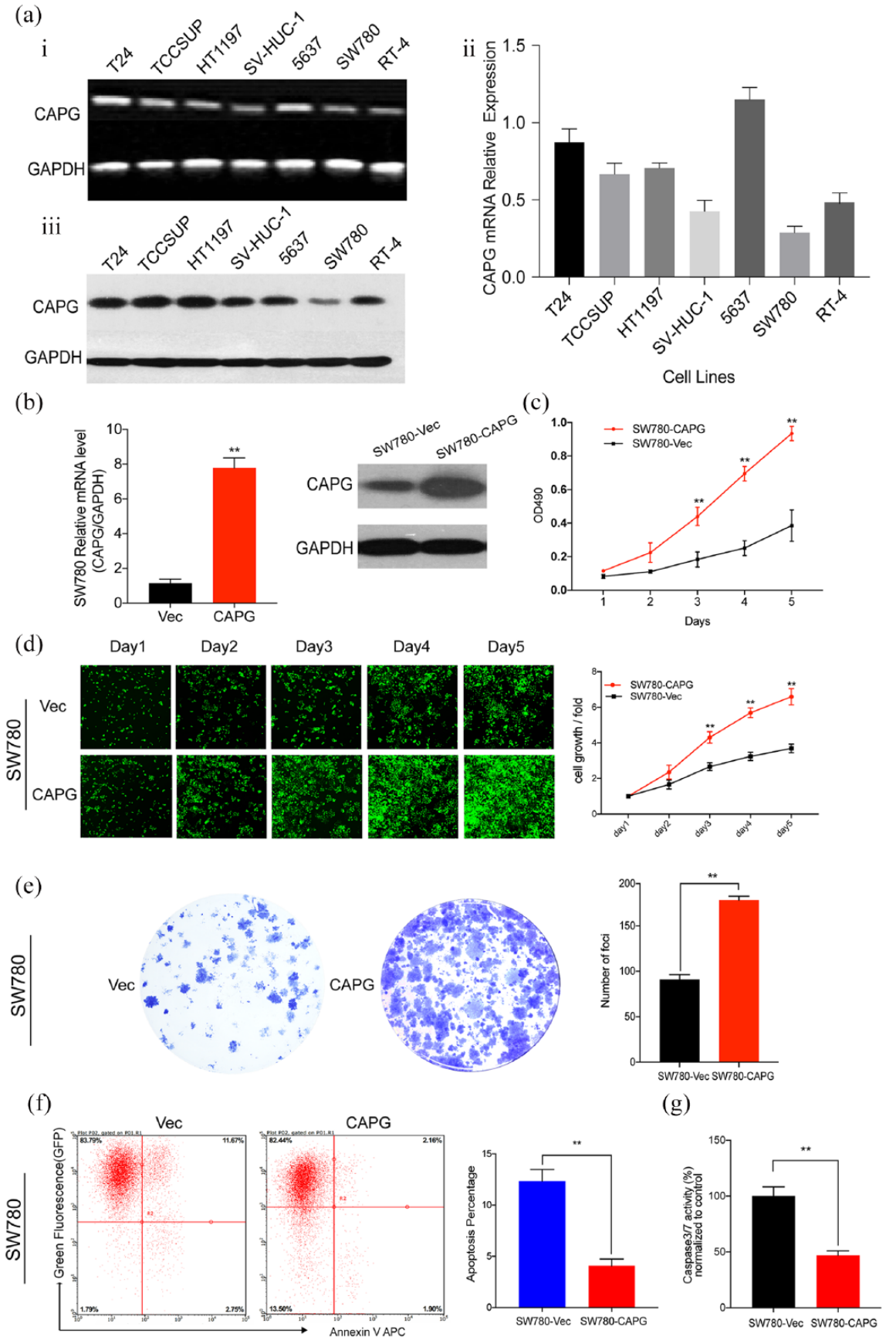

Figure 2. (Continued)

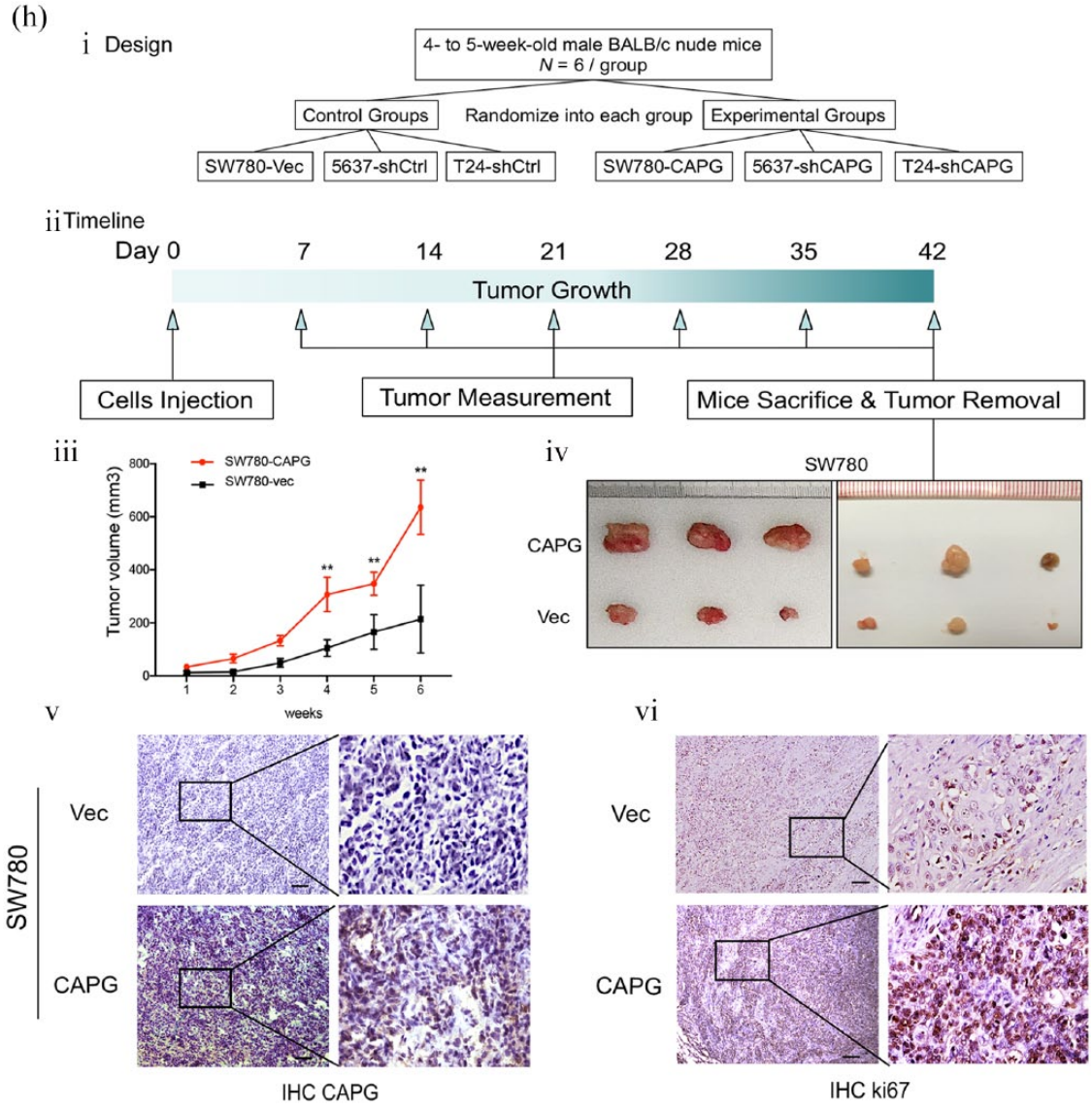

Figure 2. CAPG overexpression enhanced the tumorigenic ability in TCC cells. (a) Relative gene expression of CAPG in TCC cell lines detected by RT-PCR, qRT-PCR and western blot. GAPDH served as a loading control. (b) Overexpression of CAPG in TCC cell line SW780 was confirmed by qRT-PCR and western blot. (c) Growth curves of CAPG and vector-transfected SW780 cells detected by XTT cellular proliferation assay. (d) Representative fluorescent images (100× magnification) of SW780-Vec and SW780-CAPG cells at different time points (day 1–5) revealed by Celigo Imaging cell cytometer. The cell growth curves in the right panel indicated that CAPG overexpression significantly increased proliferation of SW780 cells. The results represent mean ± SD of three separate experiments. $^{**}p < 0.01$. (e) Representative images of foci formed by CAPG and vector-transfected SW780 cells in monolayer culture. Quantitative analysis of the number of foci are listed in the right panel. Results are presented as mean ± SD of three independent experiments. $^{**}p < 0.01$. (f and g) CAPG overexpression decreased apoptosis in TCCs. (f) Annexin V-APC single staining and flow cytometry (FACS) analysis demonstrated that the apoptosis rate was downregulated in the CAPG-overexpression group with respect to the control group in SW780 cells. (g) Caspase 3/7 activity was significantly decreased in CAPG overexpression compared with the control group. The results represent mean ± SD of three independent experiments. $^{**}p < 0.01$. (h) i and ii. The *in vivo* tumorigenesis study design and the timeline diagram of the xenograft experiment. iii. Tumor growth curves are summarized in the line chart. The average tumor volume at each time point was expressed as the mean ± SD of six mice. A Student's *t* test was used in statistics. $^{*}p < 0.05$, $^{**}p < 0.01$. iv. Representative pictures of the subcutaneous tumors formed in nude mice following injection of SW780-Vec and SW780-CAPG cells. Each group included six mice. v and vi. IHC staining of sectioned tissues with anti-CAPG and anti-ki67 antibody were presented (left: 100× magnification; right: 400× magnification).

CAPG, gelsolin-like actin-capping protein; GAPDH, glyceraldehyde 3-phosphate dehydrogenase; IHC, immunohistochemistry; qRT-PCR, quantitative Real-time Ploymerase Chain Reaction; RT-PCR, Reverse Transcription-Ploymerase Chain Reaction; SD, standard deviation; shCtrl, control cells; TCC, transitional cell carcinoma; Vec, vector.

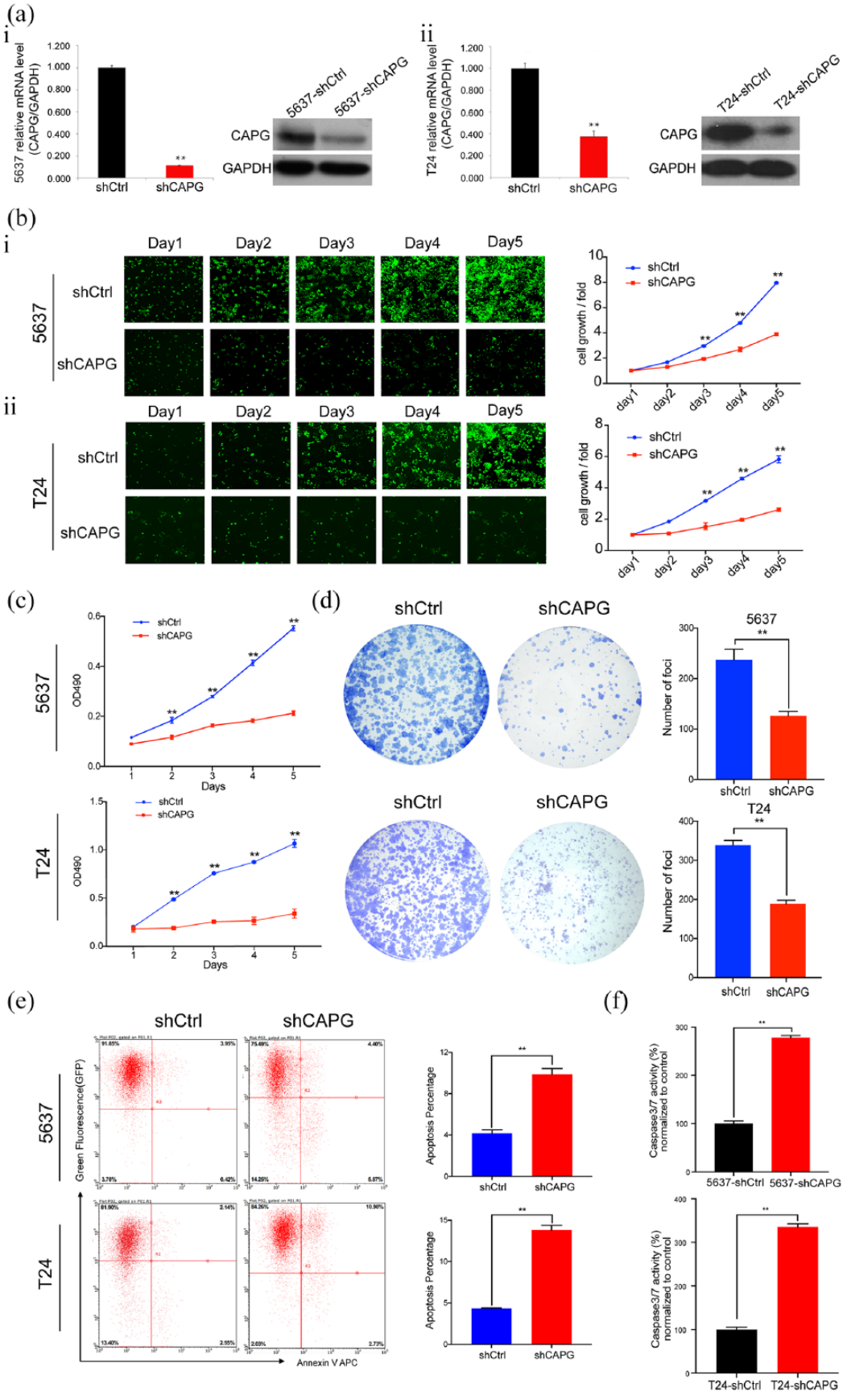

Figure 3. (Continued)

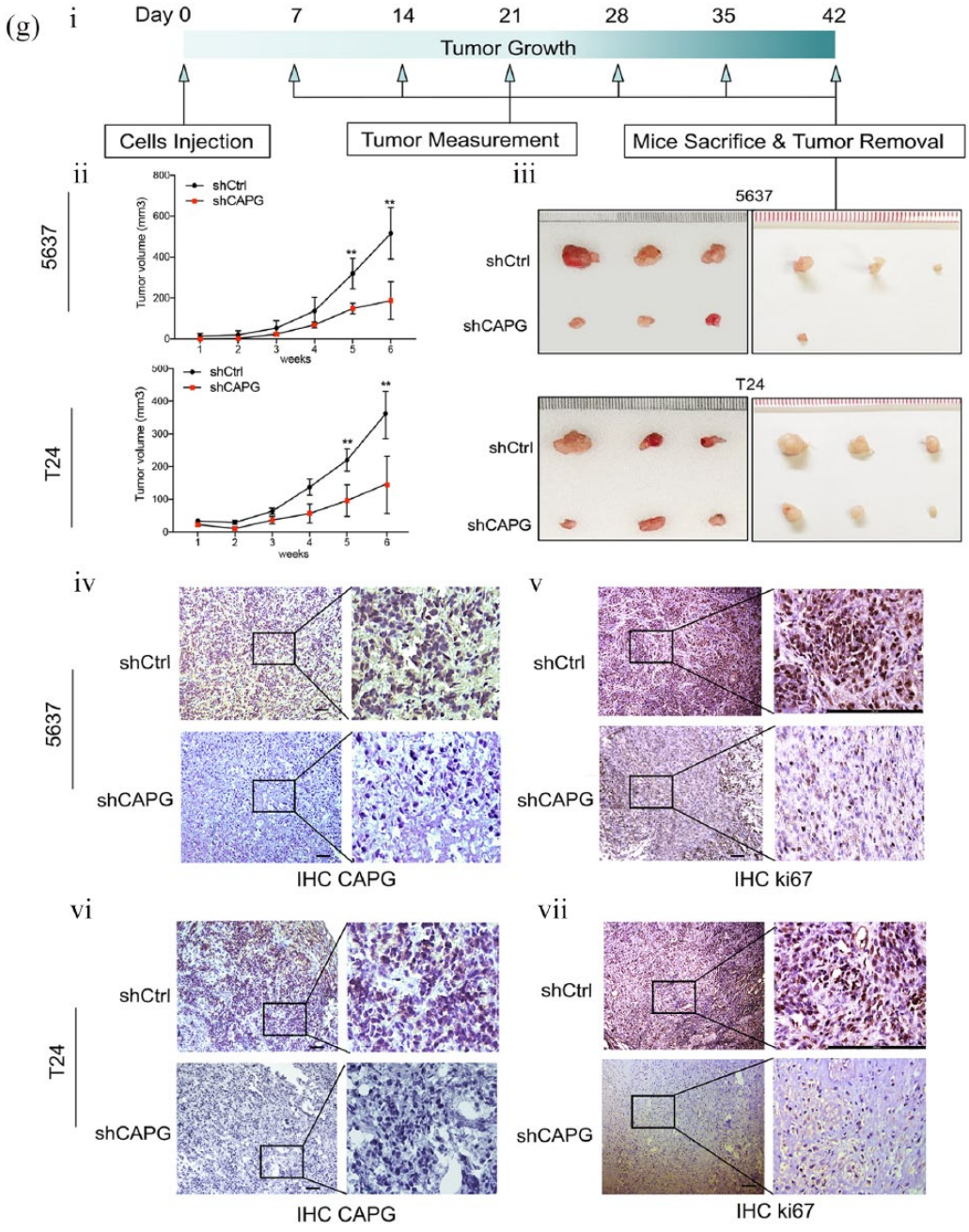

Figure 3. CAPG-knockdown attenuated TCC cells' tumorigenic ability. (a) qRT-PCR and western blot assays revealed that shCAPG lentivirus could specifically inhibit CAPG expression at mRNA and protein level in TCC cell lines 5637 and T24. (b–d) Representative images and statistic summaries of (b) Celigo Imaging assay, (c) XTT assay and (d) foci formation assay performed in shCtrl-transfected or shCAPG transfected 5637 and T24 cells. The values indicate the mean ± SD of three independent experiments. $^{**}p < 0.01$. (e and f) CAPG-knockdown-induced apoptosis in TCCs. (e) Annexin V-APC single staining and flow cytometry (FACS) analysis revealed that the apoptosis rate was significantly upregulated in the CAPG-knockdown group with respect to the control group in T24 and 5637 cells (9.77% and 13.81% *versus* 4.37% and 4.36%). (f) Caspase 3/7 activation was significantly increased in shCAPG group in T24 and 5637 cells. The caspase 3/7 activity of shCAPG group was normalized to that of the control group. The results represent mean ± SD of three independent experiments. $^{**}p < 0.01$. (g) i. The timeline diagram of the xenograft experiment by shCtrl-transfected or shCAPG transfected 5637 and T24 cells. ii. The average tumor volume at each time point was expressed as mean ± SD in six nude mice. $^{*}p < 0.05$, $^{**}p < 0.01$. iii. Representative images of tumors formed in nude mice by subcutaneous injection of shCtrl-transfected or shCAPG transfected 5637 and T24 cells. Nude mice were sacrificed to obtain tumor tissues at the injected location. iv–vii. The IHC staining with anti-CAPG and anti-ki67 antibodies demonstrated that CAPG and ki67 expressions were decreased by knockdown of CAPG compared with the control groups in both 5637 and T24 cells (left: 100× magnification; right: 400× magnification).

CAPG, gelsolin-like actin-capping protein; IHC, immunohistochemistry; qRT-PCR, quantitative Real-time Ploymerase Chain Reaction; SD, standard deviation; shCtrl, control cells; TCC, transitional cell carcinoma.

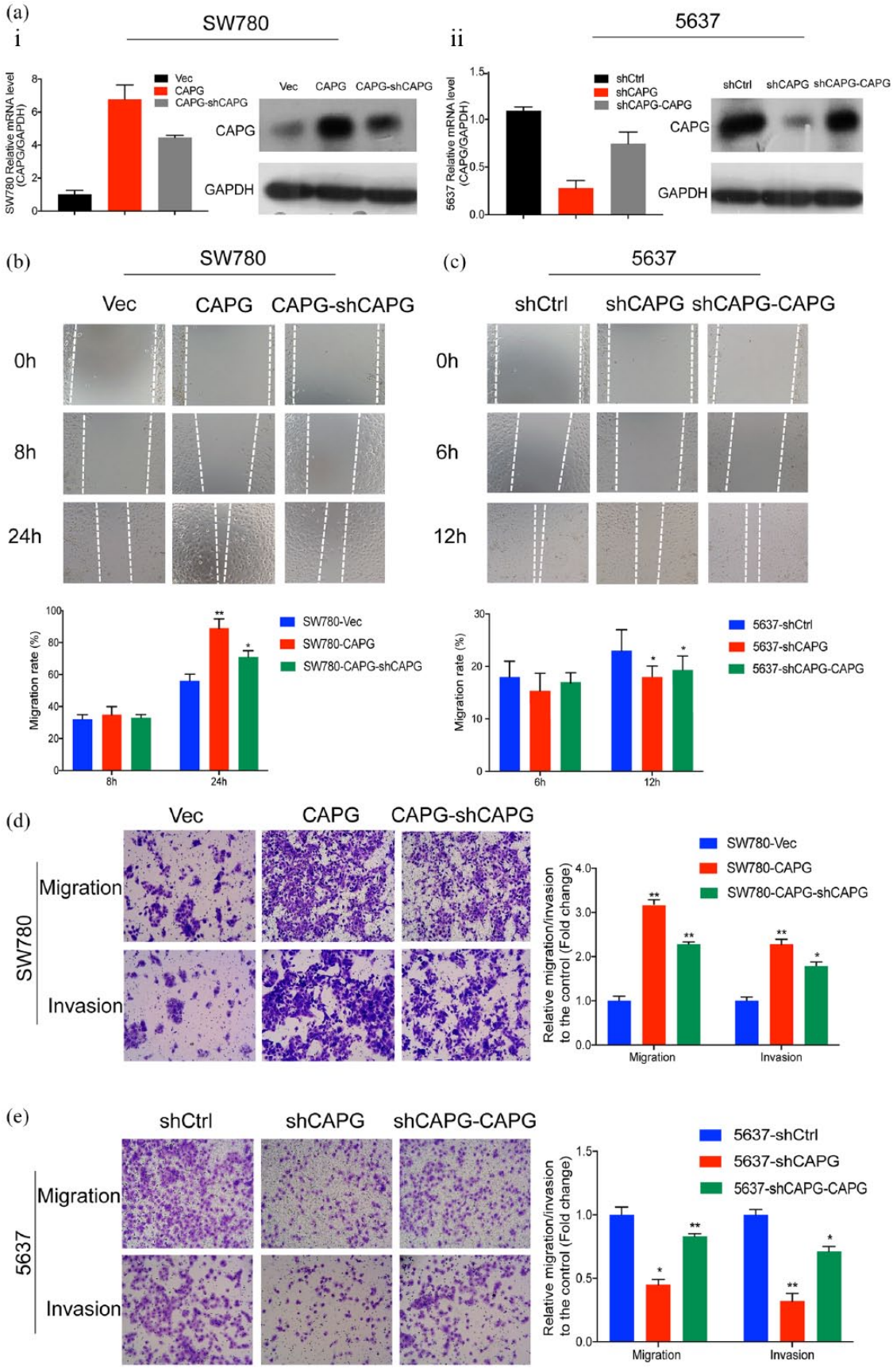

Figure 4. (Continued)

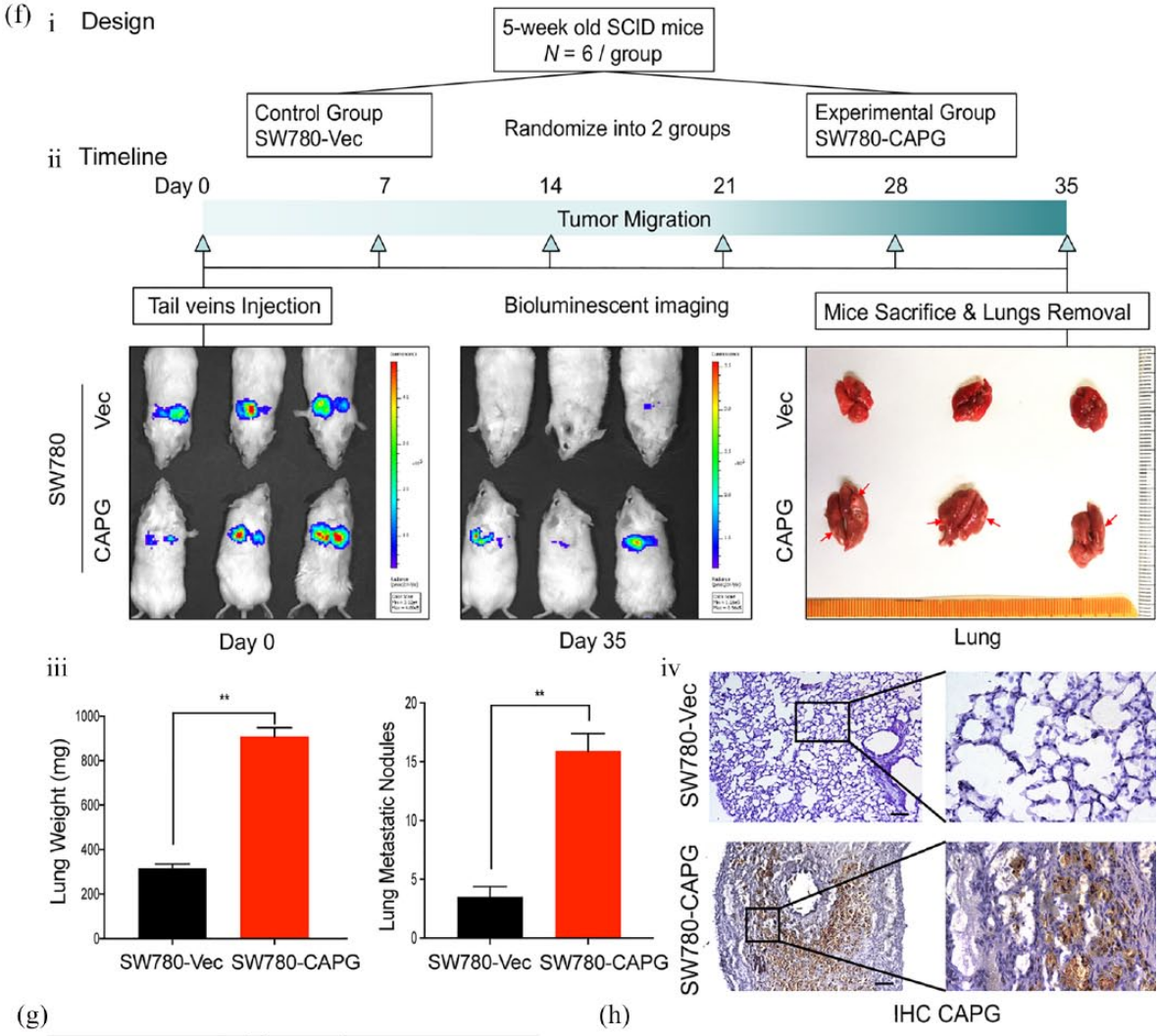

Figure 4. (Continued)

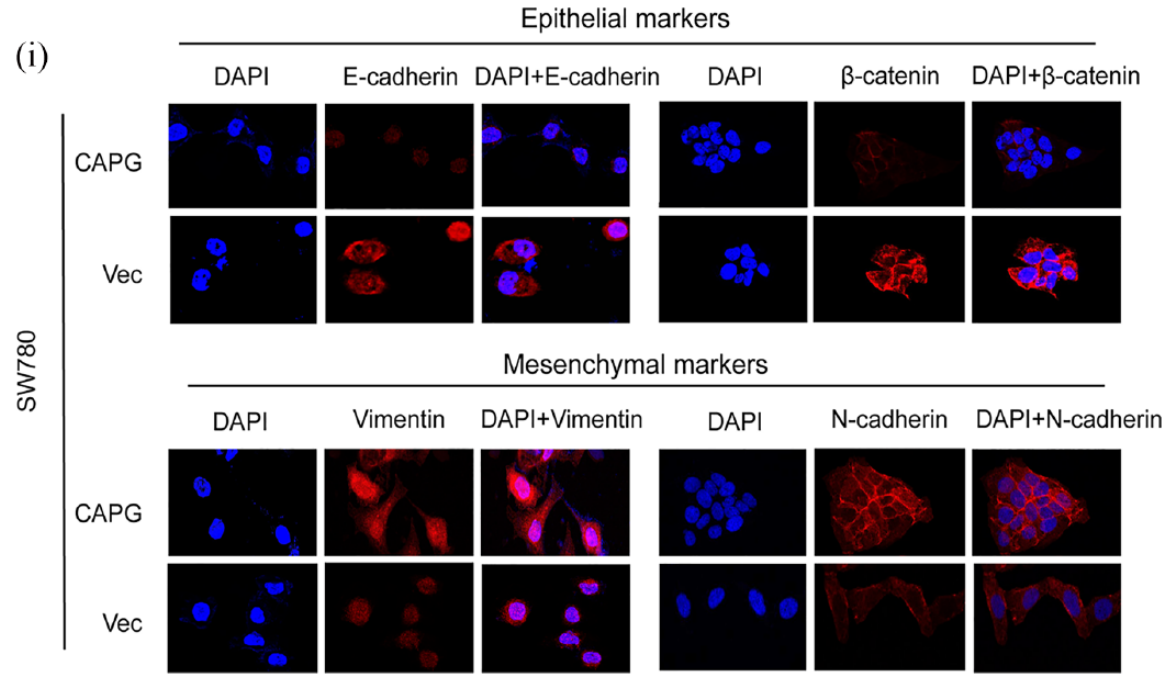

Figure 4. CAPG promotes metastasis and induces EMT in TCC cells. (a) CAPG expression level analysis by qRT-PCR and western blot in TCC (i) SW780 and (ii) 5637 cells. SW780 cells were transfected with CAPG-vector and CAPG lentivirus, and 5637 cells were infected with shCtrl and shCAPG lentivirus. After stable expression, SW780-CAPG cells were instantly infected with shCAPG plasmid; 5637-shCAPG cells were transfected with CAPG plasmid. (b and c) Representative images (upper) and quantification (lower) of the wound-healing assays. The scraping wounds which were formed by (b) SW780-Vec, SW780-CAPG and SW780-CAPG-shCAPG cells were taken at 0 h, 8 h and 24 h after wounding; formed by (c) 5637-shCtrl, 5637-shCAPG and 5637-shCAPG-CAPG cells were measured at 0 h, 6 h and 12 h under a light microscope (100× magnification). Migration rate was calculated as the ration of migration distance to the wound gap at 0 h. Migration distance of cells at 0 h was set as 0. The white dotted lines represent the wound boundary. (d and e) Representative microscopic views (left) of (d) SW780 and (e) 5637 cells which migrate through the Transwell and invade through Matrigel membrane were photographed after 24 h incubation at 100× magnification. Graphs (right) showed the fold change of the migratory and invasive cell numbers normalized to control group. Mean ± SD are shown from three independent experiments performed in triplicate for each group. Statistical significance was measured using a one-way ANOVA, $*p < 0.05$, $**p < 0.01$, $***p < 0.001$. (f) CAPG enhances TCC metastasis in the tail vein mice metastatic model. i. The *in vivo* metastatic study design. ii. The timeline diagram of the experiment. The whole bodies of mice were detected by bioluminescent imaging at day 0 and day 35, respectively. And the lungs of mice were dissected from the surrounding tissue. iii. Statistics of the measurement of lungs weight and tumor nodules. Data represent means ± SD of six mice of each group; $**p < 0.01$ by Student's *t* test. iv. IHC staining of lung sections with CAPG-antibody was taken (left, ×100 magnification and right, ×400 magnification). (g) GSEA demonstrated that EMT pathway is positively correlated with high CAPG expression. The horizontal bar in graded color from red to blue shows the rank-ordered, nonredundant list of genes. The vertical black lines represent the projection of individual genes onto the ranked gene list. Genes on the left side (red) correlated most strongly with increased EMT related gene expression. (h) Protein levels of EMT markers E-cadherin, β-catenin, vimentin and N-cadherin in CAPG-upregulated cells (SW780) and CAPG-downregulated cells (5637) and their corresponding control cells were detected by western blot assays. GAPDH served as a loading control. (i) Immunofluorescence staining of EMT markers (red) were examined in CAPG-upregulated cells SW780. Nuclei were labeled with DAPI (blue).

ANOVA, analysis of variance; CAPG, gelsolin-like actin-capping protein; DAPI, 4′,6-diamidino-2-phenylindole; EMT, epithelial-mesenchymal transition; FDR, false discovery rate; GAPDH, glyceraldehyde 3-phosphate dehydrogenase; GSEA, Gene Set Enrichment Analysis; IHC, immunohistochemistry; NES, normalized enrichment score; qRT-PCR, quantitative Real-time Ploymerase Chain Reaction; SD, standard deviation; shCtrl, control cells; TCC, transitional cell carcinoma; Vec, vector.

and the vector. The Affymetrix GeneChip Primeview arrays identified 1913 transcripts showing significantly differential expression, including 1000 upregulated and 913 downregulated genes, based on a $p < 0.05$ threshold. Differentially expressed genes were displayed in

the hierarchical clustering heatmap [Figure 5(a)] and the volcano plot [Figure 5(b)]. The enrichment analysis by IPA revealed key canonical pathways (including the Hippo, protein ubiquitination, hepatic fibrosis/hepatic stellate cell activation and unfolded protein response) and the biological functional pathways [including cellular growth and proliferation, cell death and survival, organismal survival, cellular development and cancer; Figure 5(c and d)]. Notably, the Hippo signaling was the most significantly enriched canonical pathway inactivated by CAPG ($p = 0.0001$).

The Hippo pathway is involved in a wide range of biological processes, such as organ size control, cell differentiation, tumorigenesis and cancer development.[33,34] To read out the status of the Hippo pathway regulated by CAPG in TCCs, we firstly examined the expression of the core components of Hippo using a western blot, including the cytosolic kinases: the mammalian Hippo homolog1 (MST1) and large tumor suppressor 1 (LATS1) and their coactivators: the scaffolding proteins Salvador homolog 1 (SAV1) and Mps One binder 1 (MOB1) as well as the downstream effector YAP. The overexpression of CAPG in SW780 cells decreased phosphorylation of MOB1, LATS1 and YAP, whereas the knockdown of CAPG in 5637 cells increased the phosphorylation of MOB1, LATS1 and YAP compared with the control groups [Figure 5(e)]. However, the phosphorylation of MST1 and SAV1 were not significantly changed by the regulation of CAPG. The phosphorylation of YAP causes the cytoplasmic sequestration of YAP, which could prevent its nuclear translocation and function as a transcriptional coactivator.[35,36] We therefore detected the subcellular distribution of YAP by immunofluorescence staining. CAPG-overexpressing SW780 cells had decreased levels of cytoplasmic YAP and increased levels of nuclear YAP. Conversely, knockdown of CAPG in 5637 cells reduced the nuclear localization of YAP [Figure 5(f)]. These results suggested that downregulated CAPG triggered a kinase cascade leading to phosphorylation, cytoplasmic retention and functional inactivation of YAP and vice versa.

To further delineate the key role of Hippo signaling in the tumorigenesis and metastasis regulated by CAPG, the function of Hippo was suppressed by a YAP inhibitor, VP, a compound being reported to induce sequestration of YAP in cytoplasm and interfere with YAP transcription binding effectively. VP was dissolved in DMSO (100 mg/ml), and a working solution was freshly prepared at 10 mg/ml in PBS before use. *In vitro*, CAPG-overexpressed SW780 cells were treated with VP at 1 μM/ml or 3 μM/ml and blank control (DMSO) for 24 h. The cellular location of YAP was then determined by immunofluorescence staining. As indicated in Figure 6(a), VP decreased YAP nuclear localization leading to increases in cytosolic YAP in a dose-dependent manner.

XTT assay and foci formation assay demonstrated that VP decreased the SW780-CAPG cells proliferation *in vitro*. Consistently, the inhibition of YAP abrogated the effects of CAPG on migration and invasion abilities in SW780 cells [Figure 6(b, c and d)]. The results of the *in vivo* YAP inhibition effects experiments showed that VP suppressed the tumor growth from weeks 4 compared with the control group. YAP IHC of the xenograft confirmed the YAP inhibitor decrease the nuclear expression of YAP *in vivo* [Figure 6(e)].

Taken together, these findings suggest that the tumorigenesis and metastasis caused by CAPG is associated with the Hippo pathway in TCCs (Figure 7).

Discussion

TCC is highly prevalent worldwide. It is characterized by frequent recurrence and high mortality. Unfortunately, our understanding of the genetic basis of TCC is limited, which is reflected by the absence of effective treatment modalities and prognostic markers.[37] Thus, appropriate molecular biomarkers for TCCs are needed urgently. In many other areas, actin-regulating proteins are being proposed as potential targets for drug development at a swift pace.[38] As a member of gelsolin-family, CAPG exerts important biological and physiological functions in various tissues. However, the functional characterization of CAPG in TCCs has not been studied.

Based on our findings, CAPG was highly activated in a wide variety of cancers, especially in TCCs. And the upregulation of CAPG was found to be associated with the gene copy-number amplification. Though the oncogenic function of CAPG has been reported in different cancers by investigators,[20,21,39–42] the relationship between activation of CAPG and the development of TCCs is still unknown to the best of our knowledge. In the present study, we showed for the first

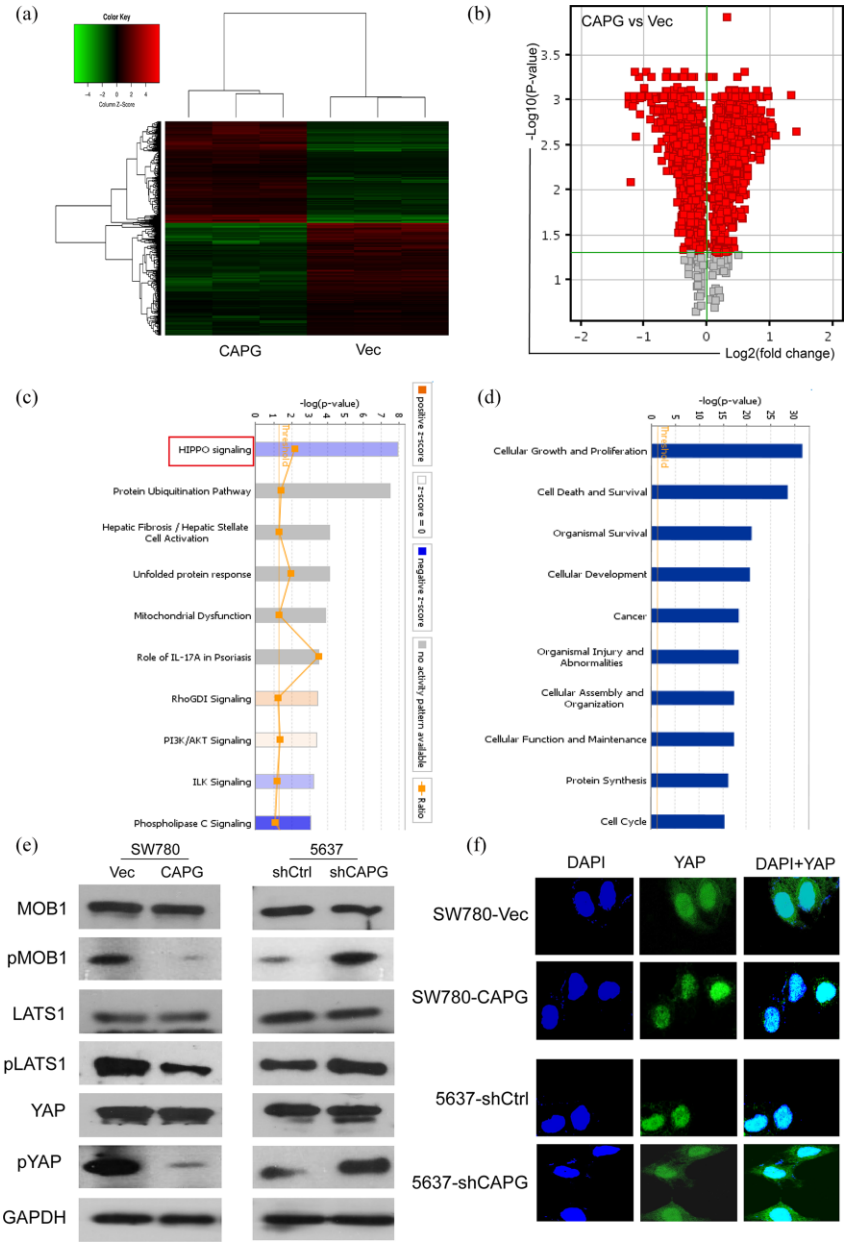

Figure 5. Regulation of Hippo signaling by CAPG. (a–d) *In silico* analysis of transcriptome and pathways mediated by CAPG (a) Hierachical clustering heat map depicting global changes of transcriptome between SW780-CAPG cells and SW780-Vec cells based on a $p < 0.05$ threshold. Rows and columns represent genes and samples, respectively. A color key for the normalized expression data is shown at top left corner of the heat map, in which red denotes upregulation, black is no difference, and green is downregulation. (b) Volcano plot presents the relationship between magnitude of gene expression changes ($\log_2$ of fold change; *x*-axis) and statistical significance of this changes ($\log_{10}$ of *p* value; *y*-axis). Red points represent differentially expressed genes with $p < 0.05$. (c) The most enriched canonical pathways analyzed by IPA. Orange and blue bars indicate predicted pathway activation (*z*-score > 0) or inhibition (*z*-score < 0). White bars are those with a *z*-score at or very close to 0. Gray bars indicate pathways that are currently ineligible for a prediction. Orange points connected by a thin line represent the ratio between the number of differential genes and the total number of genes that are in the reference gene set of a given way. (d) The biological functional pathways analyzed by IPA. The *p* value represented as negative log value (*y*-axis) is a measure of the involvement of the candidate genes in specific represented (*x*-axes) function. The threshold line represents significant *p* value of each function. (e and f) Detecting the key role of Hippo signaling regulated by CAPG in TCCs. (e) Western blot of YAP and pYAP and its upstream kinases (MOB1 and pMOB1 and LATS1 and pLATS1) in SW780 cells infected with CAPG or empty vector and 5637 cells transfected with shCAPG or shCtrl. (f) Immunofluorescent staining of YAP (green), nuclear (DAPI, blue) and their overlay in SW780-Vec or SW780-CAPG cells and 5637-shCtrl or 5637-shCAPG cells.
CAPG, gelsolin-like actin-capping protein; DAPI, 4′,6-diamidino-2-phenylindole; IPA, Ingenuity Pathway Analyses; MOB1, Mps One binder 1; LATS1, large tumor suppressor 1; Mps One binder 1; pLATS1, phosphorylated LATS1; pMOB1, phosphorylated MOB1; pYAP, phosphorylated YAP; TCC, transitional cell carcinoma; Vec, vector; YAP, Yes-associated protein.

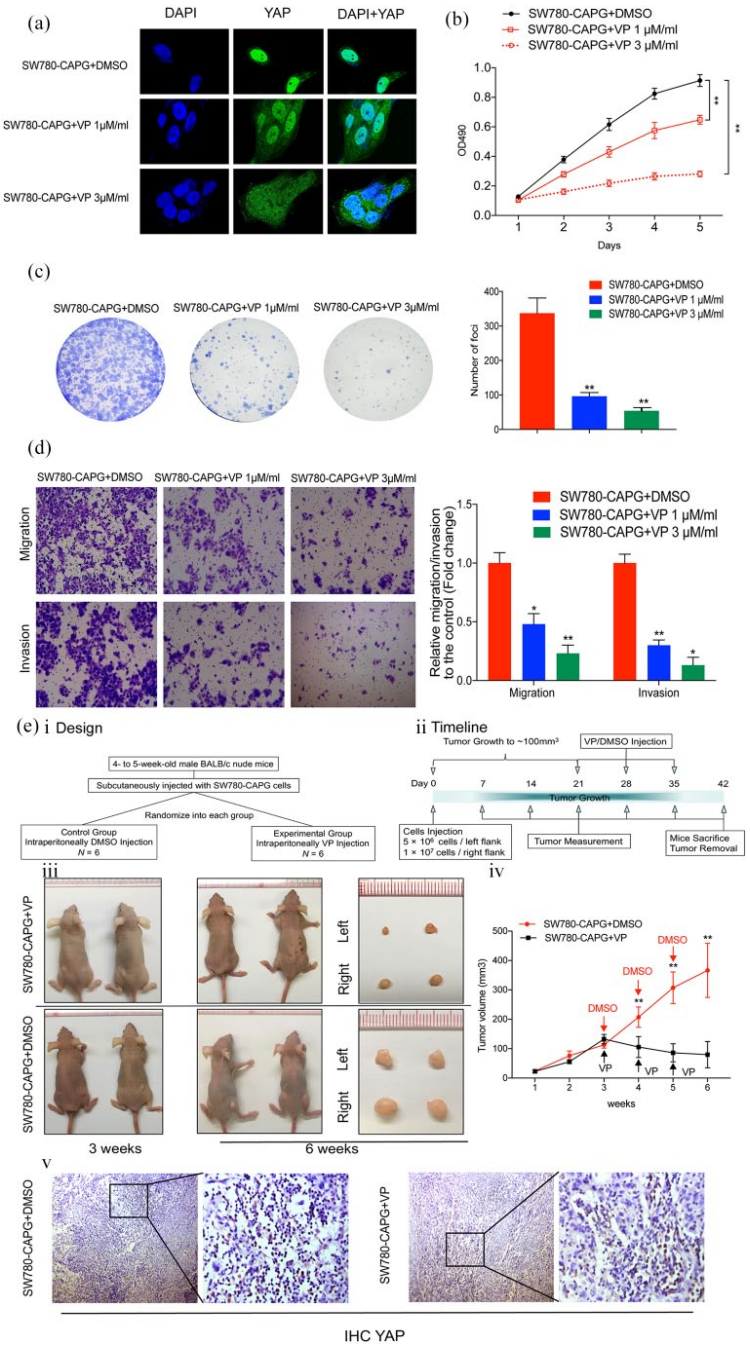

Figure 6. (a) Localization of YAP was analyzed by immunofluorescence in SW780-CAPG cells treated with VP (1 μM/ml or 3 μM/ml) or DMSO as a blank control. (b) and (c) XTT and foci formation assays revealed the role of YAP in the proliferation of CAPG-transduced SW780 cells. (d) Transwell assays revealed the inhibition of YAP decreased the migration and invasion in CAPG-overexpressed cells. (e) The xenograft mice model demonstrated that VP inhibit tumor growth regulated by CAPG through suppressing YAP nuclear translocation *in vivo*. i and ii. The *in vivo* study design and the timeline diagram. iii. The representative pictures of the mice and tumors at week 3 and week 6. The mean volume of tumors formed by SW780-CAPG in the mice grew to ~100 mm^3 at week 3. After the injection of VP and DMSO as a control for 3 weeks, the growth of tumors on both sides of the mice was suppressed significantly by the inhibition of YAP compared with the control group. iv. The statistical data of tumor volume from week 1 to week 6. The mean ± SD of relative fold changes from triplicate experiments were plotted, with *p* values calculated by a paired Student's *t* test. $*p < 0.05$, $**p < 0.01$. v. The IHC staining of the xenograft demonstrated that the nuclear localization and expression of YAP is decreased by VP treatment compared with the control groups (left: 100× magnification; right: 400× magnification).

CAPG, gelsolin-like actin-capping protein; DMSO, dimethyl sulfoxide; IHC, immunohistochemistry; pYAP, phosphorylated YAP; SD, standard deviation; TCC, transitional cell carcinoma; Vec, vector; VP, verteporfin; YAP, Yes-associated protein.

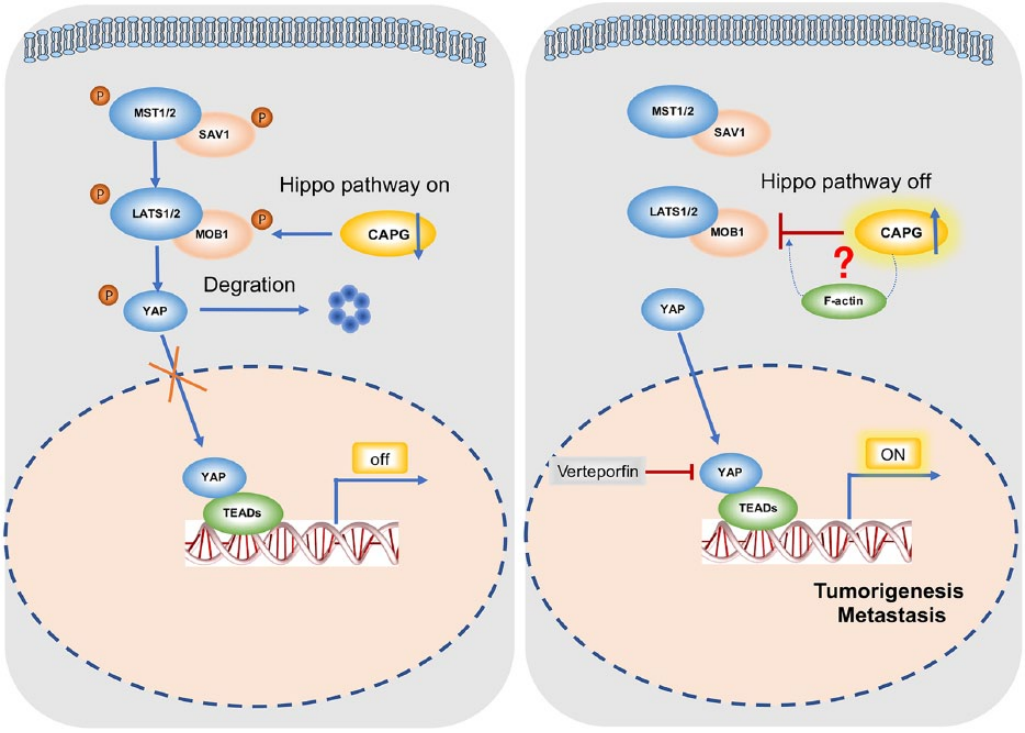

Figure 7. The schematic diagram illustrating the proposed CAPG-regulated oncogenic mechanism in TCC tumorigenesis and metastasis.
CAPG, gelsolin-like actin-capping protein; LATS1, large tumor suppressor 1; MOB1, Mps One binder 1; MST1, mammalian Hippo homolog1; SAV1, Salvador homolog 1; TCC, transitional cell carcinoma; TEAD, TEA Domain Transcription Factor; YAP, Yes-associated protein.

time the frequently upregulation of CAPG detected in clinical specimens of primary TCCs, which was significantly associated with lymph node metastasis ($p = 0.0077$), advanced pathologic stage ($p = 0.0003$) and worse prognosis ($p = 0.0080$). Thus, CAPG could be an independent prognostic factor in patients with TCCs.

The data presented here also revealed the previously undescribed findings that upregulation of CAPG led to tumorigenesis of TCCs and enhanced metastasis and EMT in TCC cells. Lymph node metastasis is the first step and the most typical pattern in the metastatic process in TCCs.[43] As a prerequisite for tumor cell invasion and metastasis, cellular mobility could be mediated by CAPG in normal cells as well as cancer cells. With the lack of cytoplasmic CAPG protein, cells fail to reorganize their actin cytoskeleton properly during motility, probably through inappropriate elongation of actin filaments. Though Sarah Tonack and colleagues suggested that the cytoplasmic CAPG may be sufficient for increased cell motility,[44] the specific ability of CAPG to enter the nucleus might also trigger the invasion .[45] The mechanism of CAPG improving cellular motility remains controversial.

EMT was shown to strongly improve cellular motility and dissemination in cancers, including TCCs.[46] It has been reported that during EMT process, activation of RhoA leads to actin cytoskeleton remodeling and disruption of E-cadherin based cell adhesions.[47] Several actin cytoskeleton-associated proteins such as α-actinin, integrins and moesin have been shown to be positively related to EMT.[48] We therefore wondered whether the cytoskeleton modulation protein CAPG could regulate EMT in TCCs. GSEA analysis on the basis of RNA-seq data from TCGA indicated that EMT signaling was significantly enriched in the CAPG-overexpression group. We next validated that the overexpression of CAPG could downregulate epithelial markers expression while upregulating the mesenchymal markers. Thus, CAPG could contribute to motility not only by cytoskeleton restructuring but also through EMT in TCC cells, which further our understanding in this regard.

In an attempt to investigate the molecular mechanisms underlying CAPG regulating tumorigenesis, a recent study reported that CAPG promoted tumorigenesis due to changes of the tumor-related proteins such as STAT4, ANK3 and IGF2.[49] Sheng Huang and colleagues reported that CAPG enhances BRCA metastasis by competing with PRMT5 to modulate STC-1 transcription.[50] Notably, in the current study, we uncovered a novel mechanism of CAPG inactivating the tumor suppressive pathway Hippo, then leading to the nuclear translocation of the oncogene YAP in TCCs. Hippo signaling is a highly conserved developmental pathway that plays an essential role in restricting organ size, tumor suppression, tissue regeneration and stem cell self-renewal.[51] The core of the Hippo pathway is a kinase cascade consisting of MST1/2 and LATS1/2. The MST1/2 kinases combined with SAV1 to activate the LATS1/2 kinases.[52] Activated MOB1-bound LATS1/2 phosphorylates YAP on serine residues, to block its nuclear import and results in inhibition of its transcriptional programs.[36] On the other hand, when the Hippo pathway is inactive, unphosphorylated YAP could translocate to the nucleus where it binds to TEA Domain Transcription Factor (TEAD) transcription factors and activate oncogenic genes. It has been reported that Hippo signaling was inactivated in human breast, prostate and colon cancer cell lines.[53] However, upstream signals that regulate the Hippo pathway are largely unknown. It has been shown that a variety of manipulations affecting the F-actin cytoskeleton can modulate the Hippo pathway.[54,55] Zhao and colleagues advanced the evidence that cell detachment and the microtubule cytoskeleton play important roles in stimulating LATS1/2 kinase activity and YAP phosphorylation.[56] Our findings suggested that CAPG overexpression inactivated the Hippo signaling through LATS1 and MOB1 dephosphorylation. Given that CAPG could regulate F-actin and the cytoskeleton, whether CAPG inactivates Hippo signaling through F-actin or other factors needs further exploration.

Conclusion

In conclusion, our data suggested a critical role for CAPG as an oncogene in TCCs and a positive relationship between CAPG and the clinical aggressiveness of patients with TCCs, which implicated the potential of CAPG as a prospective prognostic biomarker for TCCs. We further validated that the Hippo pathway had a crucial role in CAPG-mediated TCC development. The current results, together with previously reported evidence, pave the way for novel tumor diagnosis and treatment strategies with CAPG as a target for decreasing the malignant properties of TCCs.

Authors' note

Cai Zhiming is also affiliated with Carson International Cancer Center, Shenzhen University School of Medicine, Shenzhen, China.

Acknowledgements

Cai Zhiming and Wang Feng designed the study; Lyu Zhaojie, Chen Miao, Liu Yuchen, Wu Shayi, He Anbang, Zhang Meng, Liao Xinhui and Chen Yacun performed the research; Wu Peipei and Mei Hongbing analyzed the data; Lyu Zhaojie wrote the manuscript; Guan Xinyuan developed the idea for the study and commented on the manuscript.

Funding

This work was supported by the National Natural Science Foundation of China (grant number: 81602421 and 81802827) and Shenzhen Health and Family Planning Key Discipline Promotion Project (grant number: 201506026).

Conflict of interest statement

The authors declare that there is no conflict of interest.

Supplemental material

Supplemental material for this article is available online.

References

1. Siegel RL, Miller KD and Jemal A. Cancer statistics, 2018. *CA Cancer J Clin* 2018; 68: 7–30.
2. Antoni S, Ferlay J, Soerjomataram I, *et al.* Bladder cancer incidence and mortality: a global overview and recent trends. *Eur Urol* 2017; 71: 96–108.
3. Babjuk M, Böhle A, Burger M, *et al.* EAU guidelines on non-muscle-invasive urothelial carcinoma of the bladder: update 2016. *Eur Urol* 2017; 71: 447–461.
4. Mossanen M, Chang SL, Kimm S, *et al.* Current staging strategies for muscle-invasive bladder cancer and upper tract urothelial cell carcinoma. *Urol Clin North Am* 2018; 45: 143–154.

5. Mendiratta P and Grivas P. Emerging biomarkers and targeted therapies in urothelial carcinoma. *Ann Transl Med* 2018; 6: 250.
6. Creighton CJ. The clinical applications of the cancer genome atlas project for bladder cancer. *Expert Rev Anticancer Ther*, 2018; 18: 973–980.
7. Goebell PJ and Knowles MA. Bladder cancer or bladder cancers? Genetically distinct malignant conditions of the urothelium. *Urol Oncol* 2010; 28: 409–428.
8. Wu S, Lv Z, Zhu J, *et al*. Somatic mutation of the androgen receptor gene is not associated with transitional cell carcinoma: a "negative" study by whole-exome sequencing analysis. *Eur Urol* 2013; 64: 1018–1019.
9. Guo G, Sun X, Chen C, *et al*. Whole-genome and whole-exome sequencing of bladder cancer identifies frequent alterations in genes involved in sister chromatid cohesion and segregation. *Nat Genet* 2013; 45: 1459–1463.
10. Gui Y, Guo G, Huang Y, *et al*. Frequent mutations of chromatin remodeling genes in transitional cell carcinoma of the bladder. *Nat Genet* 2011; 43: 875–878.
11. Yu FX, Johnston PA, Sudhof TC, *et al*. gCap39, a calcium ion- and polyphosphoinositide-regulated actin capping protein. *Science* 1990; 250: 1413–1415.
12. Witke W, Li W, Kwiatkowski DJ, *et al*. Comparisons of CapG and gelsolin-null macrophages: demonstration of a unique role for CapG in receptor-mediated ruffling, phagocytosis, and vesicle rocketing. *J Cell Biol* 2001; 154: 775–784.
13. Van Impe K, De Corte V, Eichinger L, *et al*. The Nucleo-cytoplasmic actin-binding protein CapG lacks a nuclear export sequence present in structurally related proteins. *J Biol Chem* 2003; 278: 17945–17952.
14. Olave IA, Reck-Peterson SL and Crabtree GR. Nuclear actin and actin-related proteins in chromatin remodeling. *Annu Rev Biochem* 2002; 71: 755–781.
15. Silacci P, Mazzolai L, Gauci C, *et al*. Gelsolin superfamily proteins: key regulators of cellular functions. *Cell Mol Life Sci* 2004; 61: 2614–2623.
16. De Corte V, Van Impe K, Bruyneel E, *et al*. Increased importin-beta-dependent nuclear import of the actin modulating protein CapG promotes cell invasion. *J Cell Sci* 2004; 117: 5283–5292.
17. Nurnberg A, Kitzing T and Grosse R. Nucleating actin for invasion. *Nat Rev Cancer* 2011; 11: 177–187.
18 Sun HQ, Kwiatkowska K, Wooten DC, *et al*. Effects of CapG overexpression on agonist-induced motility and second messenger generation. *J Cell Biol* 1995; 129: 147–156.
19. Pellieux C, Desgeorges A, Pigeon CH, *et al*. Cap G, a gelsolin family protein modulating protective effects of unidirectional shear stress. *J Biol Chem* 2003; 278; 29136–29144.
20 Kimura K, Ojima H, Kubota D, *et al*. Proteomic identification of the macrophage-capping protein as a protein contributing to the malignant features of hepatocellular carcinoma. *J Proteomics* 2013; 78: 362–373.
21. Thompson CC, Ashcroft FJ, Patel S, *et al*. Pancreatic cancer cells overexpress gelsolin family-capping proteins, which contribute to their cell motility. *Gut* 2007; 56, 95–106.
22. Mosier DE, Gulizia RJ, Baird SM, *et al*. Transfer of a functional human immune system to mice with severe combined immunodeficiency. *Nature* 1988; 335: 256–259.
23. Nehls M, Pfeifer D, Schorpp M, *et al*. New member of the winged-helix protein family disrupted in mouse and rat nude mutations. *Nature* 1994; 372: 103–107.
24. Cancer Genome Atlas Research Network. Comprehensive molecular characterization of urothelial bladder carcinoma. *Nature* 2014; 507: 315–322.
25. Gao J, Aksoy BA, Dogrusoz U, *et al*. Integrative analysis of complex cancer genomics and clinical profiles using the cBioPortal. *Sci Signal* 2013; 6: pl1.
26. Rhodes DR, Yu J, Shanker K, *et al*. ONCOMINE: a cancer microarray database and integrated data-mining platform. *Neoplasia* 2004; 6: 1–6.
27. Zhang Z, Li J, Zheng H, *et al*. Expression and cytoplasmic localization of SAM68 is a significant and independent prognostic marker for renal cell carcinoma. *Cancer Epidemiol Biomarkers Prev* 2009; 18: 2685–2693.
28. Wang J, Ma Y, Zhu ZH, *et al*. Expression and prognostic relevance of tumor carcinoembryonic antigen in stage IB non-small cell lung cancer. *J Thorac Dis* 2012; 4: 490–496.
29. Slater AM and Cao L. A protocol for housing mice in an enriched environment. *J Vis Exp* 2015; e52874.
30. Cao ZA, Daniel D and Hanahan D. Sub-lethal radiation enhances anti-tumor immunotherapy in a transgenic mouse model of pancreatic cancer. *BMC Cancer* 2002; 2: 11.

31. Liu-Chittenden Y, Huang B, Shim JS, *et al*. Genetic and pharmacological disruption of the TEAD-YAP complex suppresses the oncogenic activity of YAP. *Genes Dev* 2012; 26: 1300–1305.
32. Albertson RC, Streelman JT and Kocher TD. Genetic basis of adaptive shape differences in the cichlid head. *J Hered* 2003; 94: 291–301.
33. Zhao B, Li L, Lei Q, *et al*. The Hippo-YAP pathway in organ size control and tumorigenesis: an updated version. *Genes Dev* 2010; 24: 862–874.
34. Pan D. The hippo signaling pathway in development and cancer. *Dev Cell* 2010; 19: 491–505.
35. Zhao B, Wei X, Li W, *et al*. Angiomotin is a novel Hippo pathway component that inhibits YAP oncoprotein. *Genes Dev* 2011; 25: 51–63.
36. Zhao B, Wei X, Li W, *et al*. Inactivation of YAP oncoprotein by the Hippo pathway is involved in cell contact inhibition and tissue growth control. *Genes Dev* 2007; 21: 2747–2761.
37. Masson-Lecomte A, Rava M, Real FX, *et al*. Inflammatory biomarkers and bladder cancer prognosis: a systematic review. *Eur Urol* 2014; 66: 1078–1091.
38. Van Impe K, Bethuyne J, Cool S, *et al*. A nanobody targeting the F-actin capping protein CapG restrains breast cancer metastasis. *Breast Cancer Res* 2013; 15: R116.
39. Partheen K, Levan K, Osterberg L, *et al*. Four potential biomarkers as prognostic factors in stage III serous ovarian adenocarcinomas. *Int J Cancer* 2008; 123: 2130–2137.
40. Ichikawa H, Kanda T, Kosugi S, *et al*. Laser microdissection and two-dimensional difference gel electrophoresis reveal the role of a novel macrophage-capping protein in lymph node metastasis in gastric cancer. *J Proteome Res* 2013; 12: 3780–3791.
41. Zhu WY, Hunag YY, Liu XG, *et al*. Prognostic evaluation of CapG, gelsolin, P-gp, GSTP1, and Topo-II proteins in non-small cell lung cancer. *Anat Rec (Hoboken)* 2012; 295: 208–214.
42. Shao F, Zhang R, Don L, *et al*. Overexpression of gelsolin-like actin-capping protein is associated with progression of lung adenocarcinoma. *Tohoku J Exp Med* 2011; 225: 95–101.
43. Froehner M, Novotny V, Heberling U, *et al*. Relationship of the number of removed lymph nodes to bladder cancer and competing mortality after radical cystectomy. *Eur Urol* 2014; 66: 987–990.
44. Tonack S, Patel S, Jalali M, *et al*. Tetracycline-inducible protein expression in pancreatic cancer cells: effects of CapG overexpression. *World J Gastroenterol* 2011; 17: 1947–1960.
45. Van den Abbeele A, De Corte V, Van Impe K, *et al*. Downregulation of gelsolin family proteins counteracts cancer cell invasion in vitro. *Cancer Lett* 2007; 255: 57–70.
46. Thiery JP, Acloque H, Huang RY, *et al*. Epithelial-mesenchymal transitions in development and disease. *Cell* 2009; 139: 871–890.
47. Haynes J, Srivastava J, Madson N, *et al*. Dynamic actin remodeling during epithelial-mesenchymal transition depends on increased moesin expression. *Mol Biol Cell* 2011; 22: 4750–4764.
48. Lamouille S, Xu J and Derynck R. Molecular mechanisms of epithelial-mesenchymal transition. *Nat Rev Mol Cell Biol* 2014; 15: 178–196.
49. Papala A, Sylvester M, Dyballa-Rukes N, *et al*. Isolation and characterization of human CapG expressed and post-translationally modified in Pichia pastoris. *Protein Expr Purif* 2017; 134: 25–37.
50. Huang S, Chi Y, Qin Y, *et al*. CAPG enhances breast cancer metastasis by competing with PRMT5 to modulate STC-1 transcription. *Theranostics* 2018; 8: 2549–2564.
51. Yu FX, Zhao B and Guan KL. Hippo pathway in organ size control, tissue homeostasis, and cancer. *Cell* 2015; 163: 811–828.
52. Halder G and Johnson RL. Hippo signaling: growth control and beyond. *Development* 2011; 138: 9–22.
53. Serrano I, McDonald PC, Lock F, *et al*. Inactivation of the Hippo tumour suppressor pathway by integrin-linked kinase. *Nat Commun* 2013; 4: 2976.
54. Reddy BV and Irvine KD. Regulation of Hippo signaling by EGFR-MAPK signaling through Ajuba family proteins. *Dev Cell* 2013; 24: 459–471.
55. Codelia VA and Irvine KD. Hippo signaling goes long range. *Cell* 2012; 150: 669–670.
56. Zhao B, Li L, Wang L, *et al*. Cell detachment activates the Hippo pathway via cytoskeleton reorganization to induce anoikis. *Genes Dev* 2012; 26: 54–68.